Development of a Local Hot-Cold Antenna Measurement System

by

Sean Emmanuel Manas

Thesis presented in fulfilment of the requirements for the degree of

Master of Engineering (Electronic)

in the Faculty of Engineering at Stellenbosch University

Supervisor: Dr. J. Gilmore
Co-supervisor: Dr. E. Meyer

March 2021

Declaration

By submitting this thesis electronically, I declare that the entirety of the work contained therein is my own, original work, that I am the sole author thereof (save to the extent explicitly otherwise stated), that reproduction and publication thereof by Stellenbosch University will not infringe any third party rights and that I have not previously in its entirety or in part submitted it for obtaining any qualification.

Date: 2021/03/01

Abstract

Development of a Local Hot-Cold Antenna Measurement System

S. E. Manas

Department of Electric and Electronic Engineering,
University of Stellenbosch,
Private Bag X1, Matieland 7602, South Africa.

Thesis: MEng (Electronic)

March 2021

Active antennas and antenna arrays are of great interest for high-sensitivity receiver systems, as used in radio astronomy. Several topologies for such receiver systems have low noise amplifiers closely integrated into the antenna, complicating noise measurements of sub-systems to determine the system noise temperature. This thesis presents a measurement system that can determine the system noise temperature of active antennas and antenna arrays. The developed measurement system, named Stellenbosch University Temperature Hot And COld (SU-THACO) measurement system, is deployed on the roof of the Electric and Electronic Engineering building of Stellenbosch University and operates from 1 GHz to 2 GHz. SU-THACO utilizes a graphical user interface to perform an outdoor Y-factor measurement, with the sky as the cold load and absorber material as the hot load. Radio-frequency interference is suppressed by 43.39 dBm inside the closed measurement facility, and the level of suppression is 15.19 dBm when the roof of the facility is opened. This allows for accurate noise temperature measurements in the band of interest. A successful system noise temperature measurement is completed on a commercially available active antenna, and there is reasonable agreement with the noise figure stated on the data sheet.

Opsomming

Die Ontwikkeling van 'n Antenna-ruistemperatuur Meetstelsel

S. E. Manas

Departement Elektries en Elektroniese Ingenieurswese,
Universiteit van Stellenbosch,
Privaatsak X1, Matieland 7602, Suid Afrika.

Thesis: MIng (Elektronies)

Maart 2021

Aktiewe antennas en antenna samestellings is van groot belang vir ontvangerstelsels met hoë sensitiwiteit, wat gebruik word in toepassing soos sterrekunde. Verskeie topologieë vir sulke ontvangerstelsels het laeruis versterkers wat geïntegreer is met die antenna. Hierdie hoogs geïntegreerde stelsels maak dit onmoontlik om die ruistemperatuur van individuele komponente apart te meet en die stelsel-ruistemperatuur moet dus as 'n geheel bepaal word. Hierdie tesis bied 'n meetstelsel aan wat die stelsel-ruistemperatuur van aktiewe antennas en antenna samestellings kan bepaal. Die metingstelsel, SU-THACO, is op die dak van die Elektriese en Elektroniese Ingenieurswese-gebou van die Universiteit van Stellenbosch vervaardig en opereer vanaf 1 GHz tot 2 GHz. SU-THACO word gebruik saam met 'n grafiese gebruikerskoppelvlak om buitemuurse Y-faktor metings uit te voer. Hierdie Y-faktor meting gebruik die lug as die koue-las en absorberende materiaal as die warm-las. Metings binne die geslote meetstelsel toon dat eksterne ruisbronne met 43.39 dBm onderdruk word, en as die dak van die meetstelsel afgehaal word, word die eksterne bronne met 15.19 dBm onderdruk. Dit laat metings toe met redelike sekerheid in die frekwensie gebied van die meetstelsel. Die stelsel-ruistemperatuur van 'n kommersiële beskikbare aktiewe antenna is suksesvol gemeet en daar is redelike ooreenstemming met die ruistemperatuur wat in die datablad aangehaal word.

Acknowledgements

I would like to express my sincere gratitude to the following people and organisations:

- My supervisors, Dr. Jacki Gilmore and Dr. Elmine Meyer, for their advice, guidance and proficiency throughout this project.
- My parent, for their continuous love and support.
- Lorisha, Ambre and Adam for all the encouragement and always believing in me.
- Wessel Croukamp, for his expertise, time and effort during the manufacturing.
- Gift Lecholo and Howard Koopman, for the role they played during manufacturing.
- Anneke Bester, for her assistance and expertise while doing measurements.
- My friends, for their support and understanding.
- My colleagues in the Radar Lab, for keeping me grounded.
- The NRF SARAO for funding this research.

Contents

List of Figures

List of Tables

Chapter 1

Introduction

Recent development in telescopes for radio astronomy aim to achieve high sensitivity. A metric used to express sensitivity is,

$$\text{Sensitivity} = \frac{A_{\text{eff}}}{T_{\text{sys}}}, \tag{1.1}$$

where A_{eff} is the effective collection area of the telescope and T_{sys} the system noise temperature. Thus system noise temperature is one of the main design drivers for sensitive receiver systems. [4]

During the design phase, it is sensible to know the noise contribution of each subsystem in the receiver system. However, certain topologies of integrated antenna systems have low noise amplifiers (LNAs) closely integrated to the antenna. Since they physically cannot be separated, it is impossible to measure subsystems individually. Therefore, this thesis introduces a facility that enables system noise temperature measurements of integrated antenna systems and antenna arrays.

1.1 Background

In 1887, Heinrich Hertz's experiments successfully proved the existence of radio waves, as predicted by James Clerk Maxwell's theory of electromagnetic radiation. After his discovery, unsuccessful attempts were made to measure the radio waves emitted from the sun. [5]

Forty-five years later, a radio engineer named Karl Jansky investigated the nature of static interference on trans-Atlantic radio telephone signals, leading to the discovery of a "hiss type static" from an unknown origin. [6] Through further investigation, Jansky was able to report that the Milky Way is an ample source of radio waves. [7] This led to detailed studies of extraterrestrial radio waves and is recognised as a key development in the origin of radio astronomy. [8]

In the 1990s, astronomers concluded that radio telescopes require a new level of sensitivity for improved observation, leading to the Square Kilometer Array (SKA) project, a radio telescope concept with an A_{eff} of a square kilometer. [1]

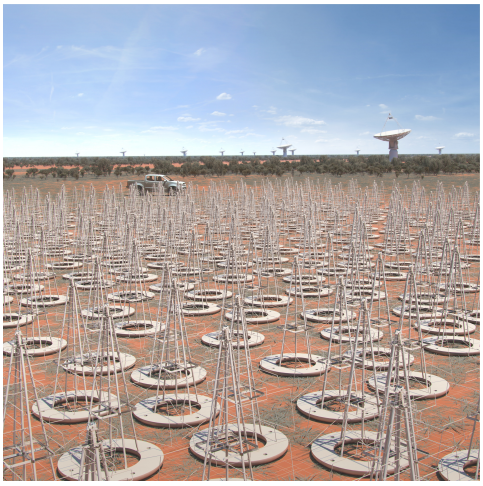

Figure 1.1: An artists rendition of SKA-low in Australia, from [1].

Figure 1.2: An artists rendition of SKA-mid reflector antennas in South Africa, from [1].

The SKA consists of an array of antennas, divided into two observing frequency ranges: the mid-frequency from 350 MHz to 15.3 GHz with the goal of 24 GHz and the low frequency from 50 MHz to 350 MHz. The construction of SKA is divided into two phases: Phase 1 (SKA1) in South Africa and Australia; with Phase 2 (SKA2) representing a significant increase in capabilities and expanding to new African countries. [9]

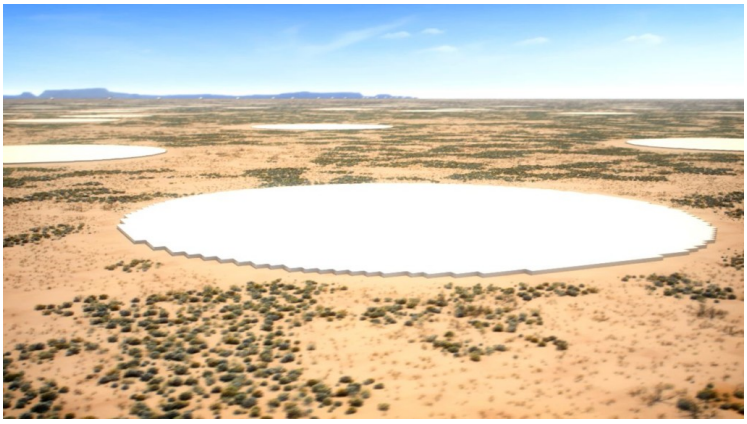

Figure 1.3: An artists rendition of SKA-mid aperture array antennas (MFAA), from [1].

The SKA1-mid telescope shown in Figures 1.2 and 1.3 will comprise of an array of reflector antennas and aperture antenna arrays. The mid-frequency aperture array (MFAA) consists of up to 10 000 small aperture antennas with LNAs closely matched to each antenna, in a 1 m^2 tile. [10–12] Phased Array Feeds (PAFs) are used to feed the mid-frequency reflector antennas. PAFs consists of hundreds of antennas and LNAs in a 1 m^2 tile, that focus on the large reflector antenna. [13, 14]

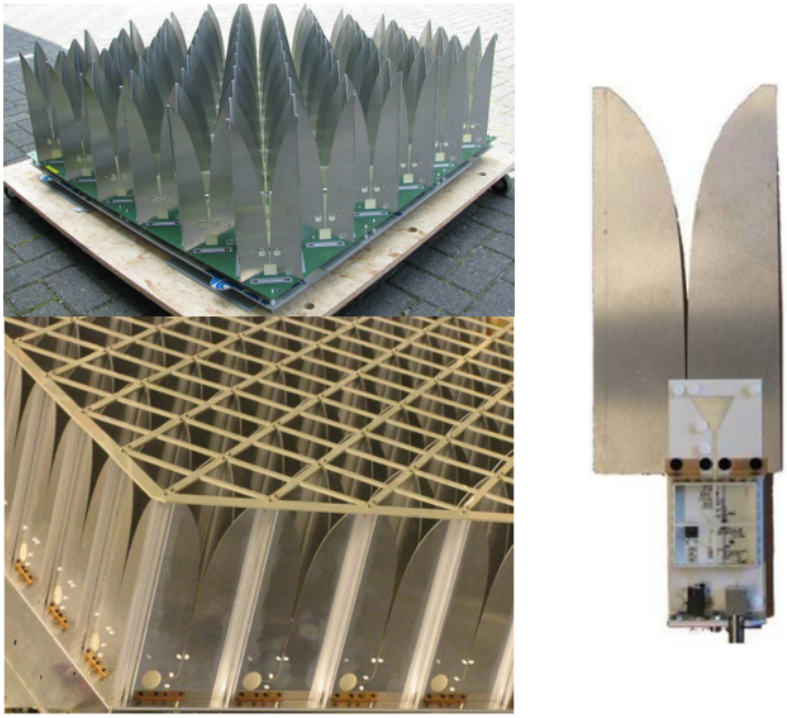

Figure 1.4: Example of 1 m^2 tiles used for MFAA and PAF (left) and a single element integrated antenna and LNA (right).

In such structures shown in Figure 1.4, gathered from [11] and [13], it is difficult to determine the system noise temperature, as the antenna and LNA cannot be physically separated. It is also difficult to measure sub-systems individually as they are noise matched, which means that not every port is terminated with the conventional 50 Ω.

Therefore, a method was introduced by Woestenburg [15,16], at the Netherlands institute for radio astronomy (ASTRON), to measure the system noise temperature of active antennas and antenna arrays through an outdoor Y-factor measurement. This measurement uses the 'sky' as the cold load and absorber material as the hot load. After seeing the influence of external noise sources, the proposal was made to develop a funnel-shaped aluminium box that enables outdoor noise temperature measurements, but suppresses noise from external sources. [2] This measurement facility is known as THACO - Temperature Hot And COld. An image of THACO is shown in Figure 1.5.

Figure 1.5: Hot-Cold measurement facility deployed at ASTRON, from [2].

The outdoor test facility delivers measurement results of the noise temperature, which is comparable and consistent with a simulation that neglects the influence of external noise contributions. [2] A study by de Vaate, Bakker and Witvers [17] has shown that having access to the facility aids the development of active antennas.

1.2 Objectives

The goal and contribution of this project is to develop a local Hot-Cold measurement system at Stellenbosch University, to measure the noise temperature of active antennas and antenna arrays. Due to the influence of radio frequency interference (RFI), the facility is aimed to operate from 1 GHz to 2 GHz. Additionally, the following minor contributions are also included:

- A study of noise found in electronic circuits, how the noise is quantified and techniques to measure the noise of devices.

- An introduction to noise contributors in a typical receiver system, which includes a study of brightness temperature to determine antenna noise temperature.
- A study on the developed noise temperature measurement facility at ASTRON.
- The development of a graphical user interface (GUI) to allow measurements with the local system to be user-friendly and repeatable.

The functionality of the facility will be proved by completing a Y-factor measurement of an active antenna. The measured results will be compared to the datasheet of the device under test, to indicate the accuracy that can be obtained with the local measurement system.

1.3 Overview

Chapter 2 discusses the fundamentals of noise in high-frequency electronic devices. Noise temperature and noise figure are defined in this chapter. In addition, an introduction to techniques of measuring the noise temperature of devices is given. Chapter 3 presents a study of the noise temperature and contributors in a typical receiver system. The contribution from the antenna and LNA is focussed on. The design of the hot-cold measurement facility deployed at ASTRON is discussed in chapter 4. In this chapter, the design process to develop a similar system on Stellenbosch University grounds is also discussed. Chapter 5 shows the results obtained from the measurement facility in Stellenbosch, whereafter a conclusion of the work is provided in chapter 6.

Chapter 2

Noise in Electronic Circuits

2.1 Introduction

Noise is defined as any random disturbance which corrupts a desired signal and reduces the certainty with which an observation or measurement may be made. [18] To evaluate these random disturbances, noise signals are considered to be stochastic and band limited around a stationary frequency, f_0, with a random amplitude, $A(t)$, and phase, $\phi(t)$, formulated as, [19]

$$i(t) = A(t)e^{j(2\pi f_0 t + \phi(t))}. \tag{2.1}$$

The stochastic nature of the noise signal means that its average value is zero and the auto-correlation of the noise signal at $t = 0$ is, [19]

$$< ii^* > = \lim_{T\to\infty} \frac{1}{T} \int_{-T/2}^{T/2} i(t+\tau)i^*(\tau)\, d\tau = \overline{i^2}, \tag{2.2}$$

which is equivalent to the mean square value of the signal. The result of the auto-correlation of the noise signal in equation 2.2 is also equivalent to the power spectral density $S_{ii}(f)$ of the signal, integrated over the frequency band,

$$< ii^* > = \int_{-\infty}^{\infty} S_{ii}(f)\, df. \tag{2.3}$$

This means that the total average power of a noise signal is equal to the auto-correlation of the signal and can be represented by the mean square value. [19]

In this chapter, different types of noise found in electronic circuits are discussed. Thereafter, a definition is given for equivalent noise temperature and noise figure. Methods used to measure the noise temperature of devices are also discussed.

2.2 Sources of Noise

In 1918, Dr Walter Schottky published his research on spontaneous current fluctuations in high-vacuum thermionic amplifiers [20], where he identified two sources of noise that are fundamental, namely, thermal and shot noise. [21]

2.2.1 Shot Noise

Schottky defined shot noise as the random fluctuation of plate current in a vacuum tube due to the arrival of charge-carrying electrons. Schottky conducted his experiments under two significant simplifying assumptions: firstly, that the transmission of an electron from the cathode to the anode of the vacuum tube happens instantly, and secondly, that only the electrostatic force between the cathode and the anode of the vacuum tube, acts on the electron. [21] The definition is formulated per unit bandwidth as

$$\overline{i_{\mathrm{S}}^2} = 2qI_{\mathrm{DC}}, \tag{2.4}$$

where $q = 1.602 \times 10^{-19}$ coulomb is the charge of an electron and I_{DC} the direct current (DC) flowing in the vacuum tube.

2.2.2 Thermal Noise

Schottky defined thermal noise as the voltage fluctuation generated by electric current flowing through a resistor at the input of the amplifier. [21] The current in the conductor is due to a spontaneous and random electric charge generated by the heat motion of its molecules. Schottky claimed that the effects of thermal noise is much smaller than that of shot noise and could thus be neglected. Engineers and physicists accepted this claim which delayed the recognition of the technical importance of thermal noise by approximately a decade. [21]

It was until 1927 when John B. Johnson found that the thermal noise level changes relative to the magnitude of resistance and absolute temperature of a conductor. [22] Johnson discussed his findings with Dr Harry Nyquist, who added that Johnson's results hold with Planck's Black Body Radiation law. This law states that any black body in thermal equilibrium radiates the average energy

$$\overline{W} = \frac{hf}{e^{hf/kT} - 1}, \tag{2.5}$$

where $h = 6.626 \times 10^{-34}$ J·s is Planck's constant, $k = 1.38 \times 10^{-23}$ J/K Boltzmann's constant, f the frequency and T the temperature in Kelvin. [23] At microwave frequencies the above equation is simplified, as $hf \ll kT$. Using the first two terms of a Taylor series expansion for the exponential gives,

$$e^{hf/kT} - 1 \simeq \frac{hf}{kT}, \tag{2.6}$$

which leads to equation 2.5 being expressed as

$$\overline{W} = kT. \tag{2.7}$$

Nyquist went on to formulate the thermal effect as a voltage applied by the source to the input of an amplifier as

$$\overline{v_{\mathrm{T}}^2} = 4kTR, \tag{2.8}$$

where $\overline{v_{\mathrm{T}}^2}$ is the mean square noise fluctuation per unit bandwidth, R the resistance, T the temperature in Kelvin and k is Boltzmann's constant. [21]

2.2.3 Other Sources of Noise

Though thermal and shot noise was described by Schottky as the dominant sources of noise in an electronic circuit, they were not the only effects observed. Another notable source of noise is the flicker effect. [21]

Flicker noise, also known as $1/f$ noise is a random process defined by the shape of its power spectral density

$$S(f) = \frac{1}{f^{\alpha}}, \tag{2.9}$$

where $0 < \alpha < 2$. [24] Flicker noise is observed as fluctuating voltage and current signals in electronic circuit components, with its effect prominent at low-frequencies.

Noise can also be generated by an external source and introduced to the electronic circuit by an antenna or through electromagnetic coupling. These external noise sources are grouped into two categories: man-made noise sources, such as motors, switches and radio transmitters; and noise caused by natural disturbances, such as lightning and sunspots. [25]

2.3 Equivalent Noise Temperature

As shown in the previous section, noise power is a result of random processes. Although the noise may be generated by various different sources, it can always be characterized in terms of noise temperature or noise figure, as long as the noise is relatively flat over the bandwidth of the system. [26, Ch. 10]

Consider a resistor at temperature T, as a thermal noise source. With equation 2.8, the voltage generated at the terminals of the resistor can be expressed as

$$V_n = \sqrt{4kTBR}, \tag{2.10}$$

where k is Boltzmann's constant, T the temperature of the resistor, B the bandwidth of the system, and R the resistance.

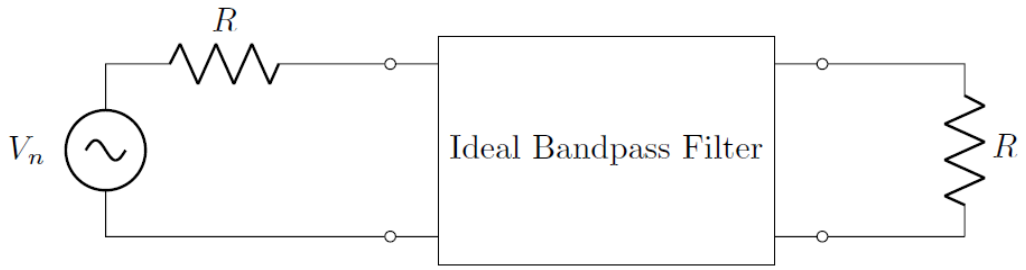

Figure 2.1: Equivalent circuit of a noisy resistor delivering maximum power to a load resistor through an ideal bandpass filter.

Consider a noiseless resistor connected to a voltage source as defined in equation 2.10, as seen in Figure 2.1. When connecting a load resistor R, it results in the maximum power transfer over a bandwidth B, [26, Ch. 10, p. 499]

$$P_n = \left(\frac{V_n}{2R}\right)^2 R = \frac{V_n^2}{4R} = kTB. \tag{2.11}$$

Equation 2.11 provides the maximum noise power from the noise resistor at temperature T. The noise power is independent of frequency and directly proportional to the bandwidth. Such a noise source has a constant power spectral density across the applicable bandwidth, and is known as a white noise source.

If an arbitrary source of noise is "white", so that the noise power is not a strong function of frequency over the bandwidth of interest, it can be modelled as an equivalent thermal noise source and characterise by an equivalent noise temperature. [26, Ch. 10, pp. 499-500]

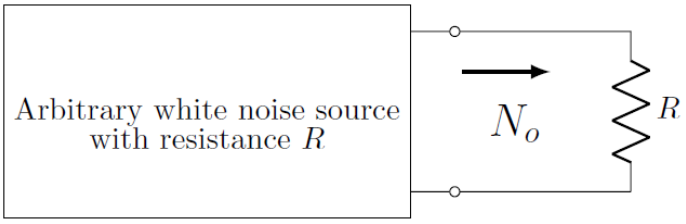

Figure 2.2: Arbitrary white noise source delivering power to a load resistor R.

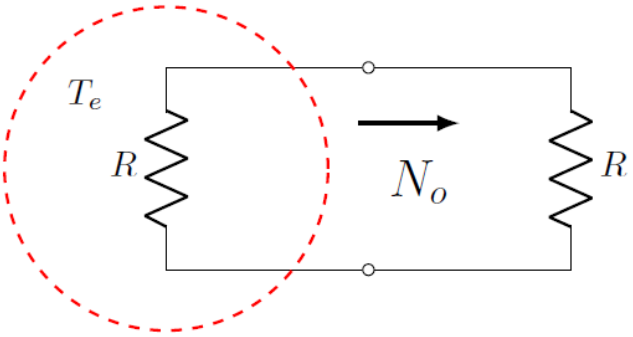

Figure 2.3: Equivalent representation of an arbitrary white noise source delivering power to a load resistor R.

Consider an arbitrary noise source, which has a driving-point impedance of R and delivers the power N_o to a load resistor R. This noise source, as seen in Figure 2.2, can be replaced with a noisy resistor of value R, at the temperature T_e, as shown in Figure 2.3. The equivalent temperature T_e represents the temperature of the source to deliver the same noise power to the load. With

$$P_n = kT_eB = N_o, \tag{2.12}$$

the equivalent noise temperature is determined as

$$T_e = \frac{N_o}{kB}. \tag{2.13}$$

Consider a system with gain G, bandwidth B, and equivalent noise temperature T_e. If the input noise power is $N_i = kT_0B$, where $T_0 = 290$ K is the reference noise temperature, the output noise power is the sum of the internal generated noise and amplified input noise power: $N_o = kGB(T_0 + T_e)$. [26, Ch. 10, pp. 503-504]

Components and subsystems in electronic circuits can thus be characterised by an equivalent noise temperature, T_e, over the operational bandwidth, B, of the component or subsystem.

2.4 Noise Figure

The noise figure is an alternative figure of merit to characterise the noise of a component. It is important to have maximum signal-to-noise ratio at the output terminal of a device. For a noiseless network, the maximum signal-to-noise ratio at the output terminal is the same as the signal-to-noise ratio at the input terminal. In general, devices add noise to the system, which reduces the signal-to-noise ratio.

Harold Friis defined noise figure as the relationship between the signal-to-noise ratio of the input and output terminals of a device, [27]

$$F = \frac{S_{in}/N_{in}}{S_{out}/N_{out}}, \tag{2.14}$$

$$\mathrm{NF} = 10\log_{10}(F), \tag{2.15}$$

where F is the linear term known as noise factor, and NF the logarithmic term. Noise figure thus represents the degradation or decrease in signal-to-noise ratio of a signal as it passes through a device. [26, Ch. 10, p. 502] The noise figure can also be expressed in terms of noise temperature as,

$$F = \frac{T_e}{T_0} + 1, \tag{2.16}$$

where T_e is the equivalent noise temperature of the device and T_0 the reference temperature defined as 290 K. Noise figure and noise temperature are two interchangeable characterisation properties.

2.4.1 Cascaded System Analysis

In a typical receiver system, the input signal passes through a chain of cascaded components, where each component adds noise to the system. If the noise figure of each component is known, the noise figure of the whole system can be calculated.

The network shown in Figure 2.4a has three components, having gains G_1, G_2 and G_3, and noise figures F_1, F_2 and F_3. The components also have equivalent noise temperatures T_{e1}, T_{e2} and T_{e3}. The cascaded network can be represented by an equivalent network, as shown in Figure 2.4b, that has the gain G_{cas}, noise figure F_{cas} and noise temperature T_{ecas}.

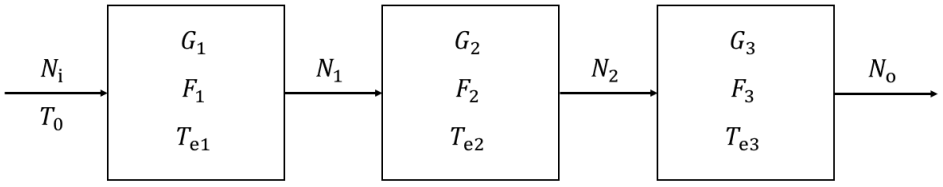

(a) Cascaded network of three elements.

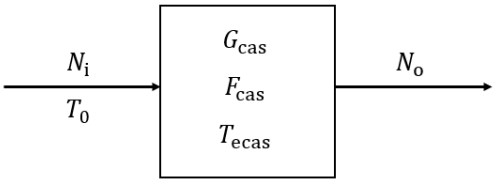

(b) Equivalent network.

Figure 2.4: Noise figure of a cascaded system.

The noise power at the output of the first stage is represented as

$$N_1 = G_1 k T_0 B + G_1 k T_{e1} B, \tag{2.17}$$

with $N_i = kT_0B$. The noise power at the second stage is expressed as

$$N_2 = G_2 N_1 + G_2 k T_{e2} B \tag{2.18}$$

$$= G_1 G_2 k B \left(T_0 + T_{e1} + \frac{1}{G_1} T_{e2} \right). \tag{2.19}$$

For the equivalent system, the output power is expressed as

$$N_o = G_3 N_2 + G_3 k T_{e3} B \tag{2.20}$$

$$= G_1 G_2 G_3 k B \left(T_0 + T_{e1} + \frac{1}{G_1} T_{e2} + \frac{1}{G_1 G_2} T_{e3} \right) \tag{2.21}$$

$$= G_1 G_2 G_3 k B (T_0 + T_{cas}), \tag{2.22}$$

which defines the noise temperature of the cascaded system as

$$T_{cas} = T_{e1} + \frac{1}{G_1} T_{e2} + \frac{1}{G_1 G_2} T_{e3}. \tag{2.23}$$

Converting noise temperature to noise figure, the noise figure of a cascaded system is given by

$$F_{cas} = F_1 + \frac{1}{G_1}(F_2 - 1). \tag{2.24}$$

Equations 2.23 and 2.24 clearly show that the equivalent representation of the cascaded system is dominated by the first stage. The second stage is reduced by the gain of the first stage, and the third stage by the gains of the first and second stage. For the best noise performance, it is important that the first stage should have low noise figure. [28] Equations 2.23 and 2.24 can be generalised to an arbitrary number of n stages:

$$T_{cas} = T_{e1} + \frac{T_{e2}}{G_1} + \frac{T_{e3}}{G_1 G_2} + \cdots + \frac{T_{en}}{G_1 G_2 \cdots G_{n-1}}, \tag{2.25}$$

$$F_{cas} = F_1 + \frac{F_2 - 1}{G_1} + \frac{F_3 - 1}{G_1 G_2} + \cdots + \frac{F_n - 1}{G_1 G_2 \cdots G_{n-1}}. \tag{2.26}$$

Equations 2.25 and 2.26 are known as Friis's formula for noise, expressed in terms of noise temperature and noise factor respectively. [29]

2.5 Measuring Noise Temperature

The equivalent noise temperature of a component can be determined if the output power is measured at 0 K. This is however not possible, because a temperature of 0 K cannot be achieved.

2.5.1 The Y-Factor Method

The Y-factor method is used to determine the equivalent noise temperature of a device under test (DUT), through the linear relationship between output noise power and input noise temperature. [26, Ch. 10, pp. 501-502]

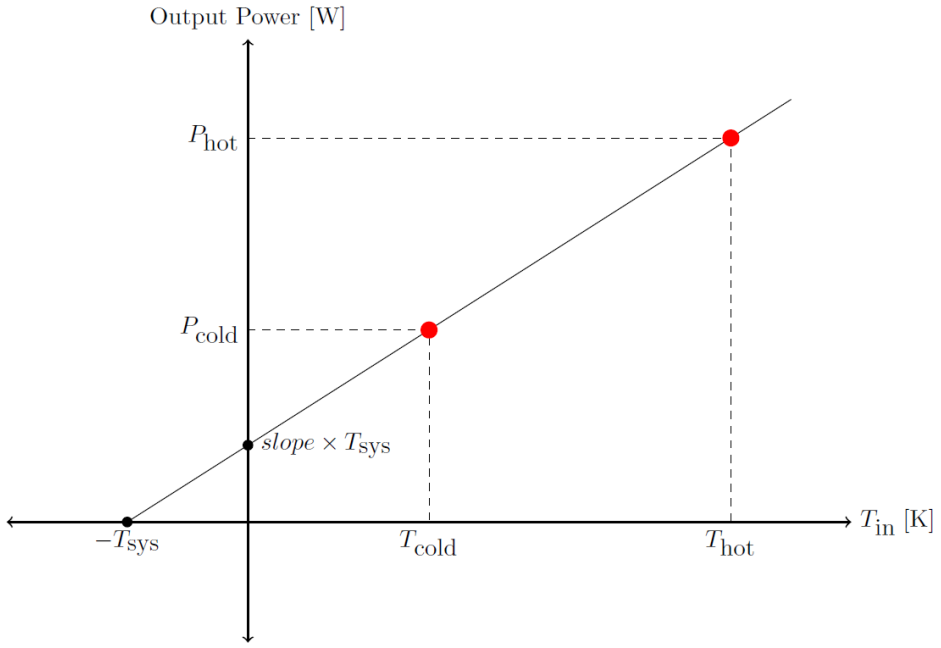

Figure 2.5: A graphical representation of the Y-factor measurement.

The method's approach is shown in Figure 2.5. The output power of the DUT at 0 K is represented by the point at '$slope \times T_{\text{sys}}$' on the y-axis. The slope of the line is expressed as

$$slope = kG_{\text{sys}}B, \tag{2.27}$$

where k is Boltzmann's constant, G_{sys} the gain of the DUT and B the bandwidth of the system. If two matched loads with a significant difference in noise temperature are used, the different output power is measured at each point and given as,

$$P_{\text{hot}} = kG_{\text{sys}}BT_{\text{hot}} + kG_{\text{sys}}BT_{\text{sys}}, \tag{2.28}$$
$$P_{\text{cold}} = kG_{\text{sys}}BT_{\text{cold}} + kG_{\text{sys}}BT_{\text{sys}}. \tag{2.29}$$

Defining the Y-factor as the ratio between the measured output powers gives

$$Y = \frac{P_{\text{hot}}}{P_{\text{cold}}}, \tag{2.30}$$

which is simplified as

$$\begin{aligned} Y &= \frac{(T_{\text{hot}} + T_{\text{sys}})kG_{\text{sys}}B}{(T_{\text{cold}} + T_{\text{sys}})kG_{\text{sys}}B} \\ &= \frac{T_{\text{hot}} + T_{\text{sys}}}{T_{\text{cold}} + T_{\text{sys}}} > 1. \end{aligned} \tag{2.31}$$

Thus T_{sys} can be solved as

$$T_{\text{sys}} = \frac{T_{\text{hot}} - YT_{\text{cold}}}{Y - 1}, \tag{2.32}$$

in terms of the load temperatures and the Y-factor. To get a reliable measurement, T_{hot} and T_{cold} must be far from each other, to avoid Y being close to unity. This is shown in Figure 2.5 and is applied through the following measurement techniques.

2.5.2 Measurement Techniques

The following measurement techniques all employ the Y-factor method to obtain noise temperature data. These techniques are discussed by Fernandez [30] and summarized below.

2.5.2.1 Standard Hot and Cold Loads

This standard method involves switching the DUT input between two different load resistors with different known physical temperatures. In practice, one load is usually a resistor at room temperature ($T_0 = 290$ K), and the other a resistor immersed in liquid nitrogen ($T = 77$ K) or liquid helium ($T = 4$ K).

2.5.2.2 Noise Temperature Measurement with a Noise Source

The simplest method for making noise temperature measurements of active devices such as amplifiers, is to use a calibrated noise source in conjunction with a noise figure meter. The noise source is switched off for the cold measurement, and switched on for the hot measurement. The hot temperature relates to the excess noise ratio (ENR) of the noise source given as,

$$ENR_{dB} = 10 \log \left(\frac{T_{source}^{on} - T_{source}^{off}}{T_0} \right). \tag{2.33}$$

Assuming the off temperature is also 290 K, the on temperature of a noise source with the ENR of 15 dB is calculated as

$$T_{source}^{on} = T_0 \left(1 + 10^{(15/10)}\right) = 9\,460.61 \text{ K}. \tag{2.34}$$

2.5.2.3 Hot-Cold Measurement inside Cryogenic Cooled Test-bed

Using a thermal noise source inside the cryogenic environment with the DUT, the source is attached to a heater. The cryogenic environment cools the DUT to a typical temperature of 15 K. First, no heat is applied to the thermal noise source and a cold measurement is taken, then the heater is turned on for a hot measurement. Repeatability is problematic for this technique since the physical temperature has to be measured when the heater is switched on for the hot measurement.

2.5.2.4 Cold Sky and Ambient Absorber Measurement

This method uses a calibrated horn antenna, with a very low side-lobe pattern to minimize ambient noise pickup from the ground. The antenna is connected to the input of the DUT, which is in a room-temperature environment. A spectrum analyser is used to measure the power difference between pointing the test antenna at the cold sky (4 K) or at ambient absorbers ($T_0 = 290$ K).

2.5.2.5 Noise Measurement with a Cryogenic Attenuator

In this technique, the cold load is provided with the noise diode switched off. The temperature applied to the DUT is equal to the cryogenic environment (15 K) plus a small contribution from the attenuated noise source (3 K). The 9 000 K noise source is then switched on and the noise power is attenuated to about 90 K to provide the hot load.

2.6 Conclusion

This chapter gives an introduction to noise in electronic circuits. Noise sources are discussed, where definitions of thermal, shot and flicker noise are given. Equivalent noise temperature and noise figure are also defined in this chapter. The analysis of a cascaded system showed the importance of minimizing the noise of the first stage amplification. Thereafter, methods to measure noise temperature is discussed. It is shown that the Y-factor method, consisting of one hot and one cold measurement, may be used to determine the system noise temperature, if the temperature of the hot and cold conditions are known. In the following chapter, the system noise temperature of a typical receiver system is elaborated on.

Chapter 3

System Noise Temperature

3.1 Introduction

The system noise temperature of a typical receiver system is defined as,

$$T_{\text{sys}} = \eta_{\text{rad}} T_{\text{A}} + (1 - \eta_{\text{rad}}) T_{\text{P}} + T_{\text{rec}} \tag{3.1}$$

where T_{A} is the antenna noise temperature, T_{P} is the physical temperature of the antenna, η_{rad} the radiation efficiency of the antenna and T_{rec} is the receiver noise temperature. Radiation efficiency is defined as the ratio of the radiated output power to the supplied input power:

$$\eta_{\text{rad}} = \frac{P_{\text{rad}}}{P_{\text{in}}} = \frac{P_{\text{in}} - P_{\text{loss}}}{P_{\text{in}}} = 1 - \frac{P_{\text{loss}}}{P_{\text{in}}}, \tag{3.2}$$

where P_{rad} is the total power radiated by the antenna, P_{in} the total power supplied to the input of the antenna and P_{loss} the power lost in the antenna. [26, Ch. 14, pp. 658-671]

This chapter elaborates on system noise temperature for a typical receiver system and related concepts, including antenna noise temperature and brightness temperature.

3.2 Antenna Noise Temperature

The IEEE standard definitions of terms for antennas, defines the noise temperature of an antenna as *the temperature of a resistor having an available thermal noise power per unit bandwidth equal to that at the antenna's output at a specified frequency.* [31]

The noise temperature of the antenna comes from noise that is generated internally and externally. The internally generated noise temperature is given by $(1 - \eta_{\text{rad}})T_{\text{P}}$. The externally generated noise temperature is defined by:

$$T_{\mathrm{A}} = \frac{\int_{\phi=0}^{2\pi}\int_{\theta=0}^{\pi} T_{\mathrm{b}}(\theta,\phi)D(\theta,\phi)\sin\theta\, d\theta\, d\phi}{\int_{\phi=0}^{2\pi}\int_{\theta=0}^{\pi} D(\theta,\phi)\sin\theta\, d\theta\, d\phi}, \tag{3.3}$$

where $T_{\mathrm{b}}(\theta,\phi)$ is the brightness temperature distribution of the surroundings of the antenna and $D(\theta,\phi)$ is the directivity of the antenna.

$$D = \frac{U_{\max}}{U_{\mathrm{avg}}} = \frac{4\pi U_{\max}}{P_{\mathrm{rad}}} \tag{3.4}$$

The directivity of an antenna is defined as the ratio of the radiation intensity in a given direction from the antenna to the radiation intensity averaged over all directions. [31]

Equation 3.3 shows that the antenna noise temperature can be interpreted as the weighted average of the brightness distribution as seen by the antenna. If a uniform source of brightness temperature T_{b} fills the entire beam pattern of the antenna, then $T_{\mathrm{A}} = T_{\mathrm{b}}$.

There are different source contributions to the brightness distributions surrounding the antenna. Firstly, there is the background temperature of the sky, secondly emissions from gases in the atmosphere and finally emissions from the ground. This section gives a condensed review on brightness temperature, based on the work done by Medellin [3]. In the scope of this thesis, focus is given to derive a sky brightness temperature model, and emissions from the ground is ignored.

3.2.1 Brightness Temperature and Radiative Transfer

Radiative transfer theory describes the intensity of radiation inside a medium, such as the atmosphere, that absorbs, emits and scatters radiation. The radiation field is described by a specific intensity, I_f [$\mathrm{W\,m^{-2}\,str^{-1}\,Hz^{-1}}$].

In the atmosphere, the radiation emitted by molecules is attenuated through atmospheric absorption. The attenuation is proportional to the distance travelled by the emitted radiation. The energy that is absorbed, is re-emitted as thermal radiation. Ignoring scattering contributions in the atmosphere, the specific intensity received in any direction is given by,

$$I_f = I_f(s_o)e^{-\tau_f(0,s_o)} + \int_0^{s_o} \kappa_a(f,s)B_f(T)e^{-\tau_f(0,s)}ds, \tag{3.5}$$

where $I_f(s_o)$ is the background intensity at distance s_o, $\kappa_a(f,s)$ the atmospheric absorption coefficient, $B_f(T)$ is the source in the medium, and τ_f is the optical depth or opacity of the medium, described as,

$$\tau_f(s_o,s) = \int_{s_o}^{s} \kappa_a(f,\xi)d\xi. \tag{3.6}$$

As the radiation is thermal, the source in the atmosphere corresponds to Planck's function,

$$B_f(T) = \frac{2hf^3}{c^2}\frac{1}{e^{hf/kT}-1}, \tag{3.7}$$

where h is Planck's constant, k Boltzmann's constant, f is the frequency and c the speed of light. At microwave frequencies, as $hf \ll kT$, the Rayleigh-Jeans approximation then describes,

$$B_f(T) \approx \frac{2kT}{\lambda^2}. \tag{3.8}$$

The linear dependence of equation 3.8 to the physical temperature, T, allows the brightness temperature to be defined as,

$$T_b = \frac{\lambda^2}{2k} I_f. \tag{3.9}$$

Equation 3.5 can now be rewritten as,

$$T_b(f) = T_{bo}(f)e^{-\tau_f(0,s_o)} + \int_0^{s_o} \kappa_a(f,s)T(s)e^{-\tau_f(0,s)}ds, \tag{3.10}$$

where $T_{bo}(f)$ is the background brightness temperature due to cosmic emissions.

3.2.2 Atmospheric Absorption

Atmospheric absorption at microwave frequencies, are dominated by two sources, namely water vapour (H_2O) and oxygen (O_2). [3] The two main effects of O_2 and H_2O on atmospheric absorption, is firstly, at tropospheric high pressure spectral lines broadens and the atmospheric transition of O_2 and H_2O spans several gigahertz. Secondly, water vapour is the dominant source of attenuation at microwave frequencies. Thus the atmospheric absorption coefficient for microwave frequencies can be expressed as,

$$\kappa_a(f,s) = \kappa_{\mathrm{H_2O}}(f,s) + \kappa_{\mathrm{O_2}}(f,s). \tag{3.11}$$

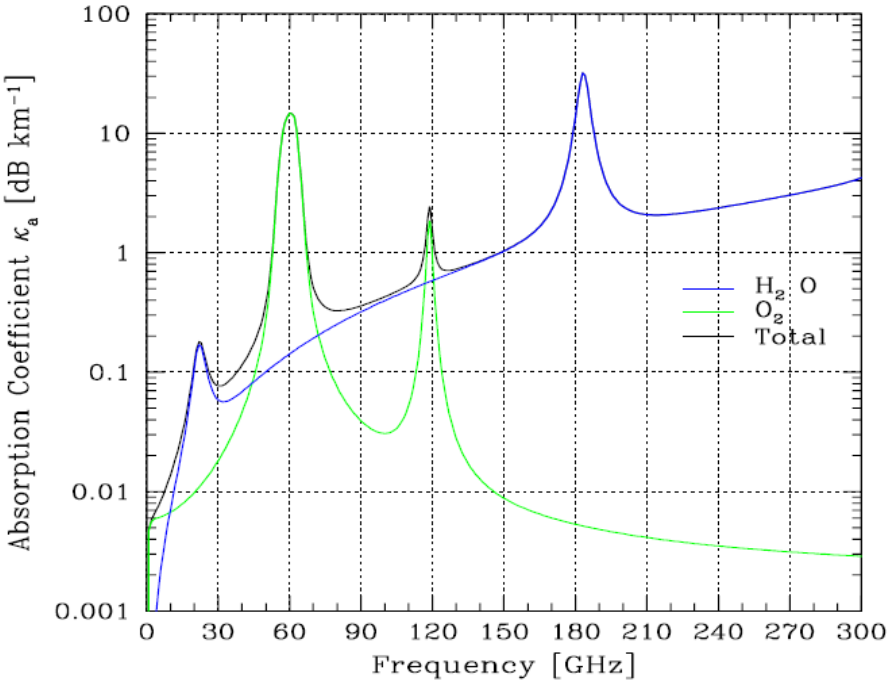

Figure 3.1: Atmospheric absorption at microwave frequencies due to H_2O and O_2, from [3].

Figure 3.1 shows the atmospheric absorption model presented by Medellin [3], which follows the work done by Ulaby [32]. This model comprises of two simpler models to calculate the atmospheric absorption of water vapour and oxygen molecules at microwave frequencies, as presented by Waters [33] and Rosenkranz [34].

The atmospheric absorption coefficient in Figure 3.1 is calculated at sea level conditions. The O_2 absorption consists of a single line absorption at 118.75 GHz, and a large number of absorption lines spanning from 50 GHz to 70 GHz, which forms an absorption band centred around 60 GHz. H_2O has two important absorption lines at 22.235 GHz and 183.31 GHz.

3.2.3 Cosmic Emissions

The background brightness temperature, $T_{bo}(f)$, can be reduced to two terms,

$$T_{bo}(f) = T_{\text{CMB}} + T_{\text{gal}}(f), \tag{3.12}$$

where $T_{\text{CMB}} = 2.73$ K is the cosmic microwave background emission and $T_{\text{gal}}(f)$ the galactic emission, which follows a power spectrum law:

$$T_{\text{gal}}(f) = T_{g_o}\left(\frac{f_o}{f}\right)^{\beta}, \tag{3.13}$$

where T_{g_o} is the base temperature and β the spectral index, which is dependent on the direction of observation in the sky. T_{g_o} varies from a minimum of 3 K

to a maximum of 507 K in the direction of the galactic centre. The value of β also varies between 2.5 in the direction of the galactic centre to 3.2 within a region above the galactic plane.

Medellin [3] uses the average value of $\beta = 2.75$, with $T_{g_o} = 20$ K at $f_o = 0.408$ GHz to obtain reasonable results for galactic noise contributions for frequencies above 10 MHz. The calculated $T_{bo}(f)$ term, under these approximations, is plotted in Figure 3.2.

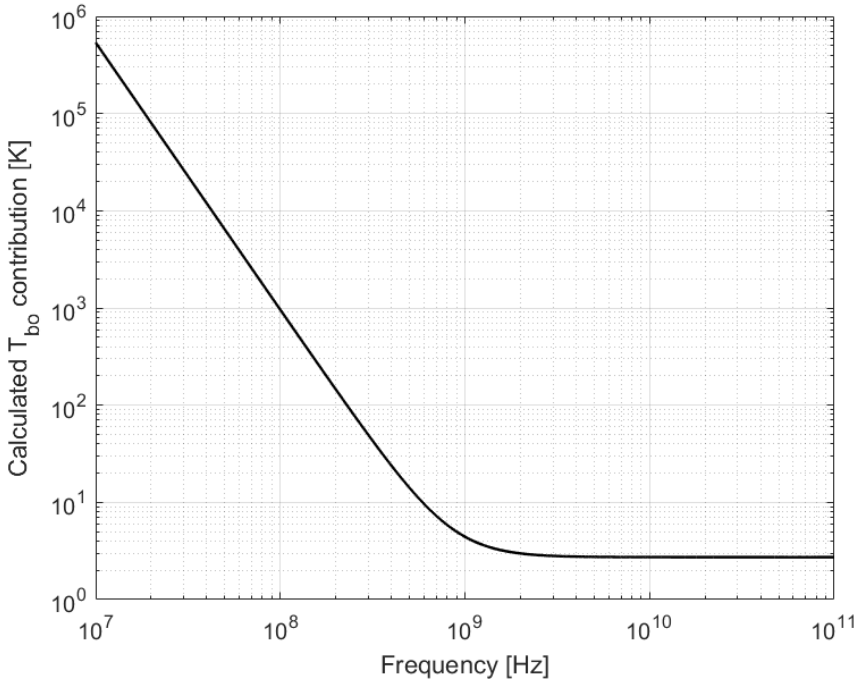

Figure 3.2: Calculated noise temperature contribution due to cosmic emissions for microwave frequencies.

3.2.4 Simplified Sky Brightness Temperature Model

Ground-based observations has a defined observation angle, θ, with respect to the zenith. Taking this into consideration, equation 3.10 can be defined as sky brightness temperature measured from the ground, which is given as,

$$T_b^{\text{sky}}(f,\theta) = T_{bo}(f)e^{-\tau_f(0,\infty)\sec\theta} + \sec\theta \int_0^\infty \kappa_a(f,s)T(s)e^{-\tau_f(0,s)\sec\theta}ds, \quad (3.14)$$

where $T_{bo}(f)$ is the background brightness temperature, given by equation 3.12 and $\tau_f(0,\infty)$ the opacity of the atmosphere at zenith, defined as,

$$\tau_f(0,\infty) = \int_0^\infty \kappa_a(f,\xi)d\xi. \quad (3.15)$$

Taking into account the contributions from the atmosphere and cosmic emission at microwave frequencies, as discuss in the two subsections above, $T_b^{\text{sky}}(f, \theta)$ can be calculated for different θ angles with respect to zenith.

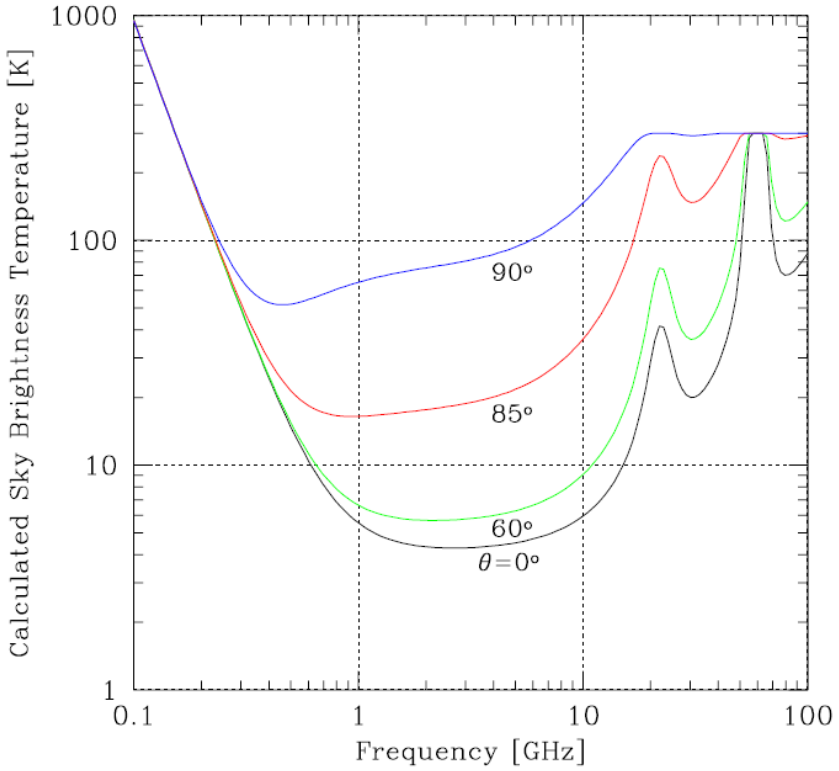

Figure 3.3: Calculated sky brightness temperature as a function of frequency, from [3].

Figure 3.3 shows the calculated sky brightness temperature at different θ angles, from [3]. Assume an antenna pointed in a direction towards the sky, and emissions from the ground can be ignored, then the sky brightness temperature is used as the $T_{\text{b}}(\theta, \phi)$ term in equation 3.3 to calculate the antenna noise temperature.

3.3 Receiver Noise Temperature

The receiver noise temperature, T_{rec}, is the effective noise temperature of the entire receiver system referenced to the antenna terminal. This includes the noise contribution from all components, noise due to mismatches and all transmission line losses, with the main contributor being the noise from the first stage LNA. [35]

The noise due to the LNA, T_{LNA}, is dependent on the noise properties of the LNA. Standard parameters that define noise in a component are:

- minimum noise temperature - T_{min}
- optimum reflection coefficient - Γ_{opt}
- noise resistance - R_{n}

The LNA noise temperature can be given as, [26, Ch. 12, 580-581]

$$T_{\text{LNA}} = T_{\text{min}} + \frac{4T_0R_{\text{n}}}{Z_0}\frac{|\Gamma_{\text{s}} - \Gamma_{\text{opt}}|^2}{|1 + \Gamma_{\text{opt}}|^2 (1 - |\Gamma_{\text{s}}|^2)}, \tag{3.16}$$

where Γ_{s} is the reflection coefficient at the input terminal of the LNA.

3.4 Conclusion

This chapter gives an overview of the system noise temperature of a receiver system, which is defined in equation 3.1 as a combination of two factors: the noise contribution from the antenna and the noise contributions from components in the receiver system. The antenna noise temperature is then defined as noise that is generated internally and externally from the antenna. The internally generated noise is dependant on the physical temperature of the antenna, while the externally generated noise is calculated from the brightness temperature distribution surrounding the antenna. A simplified sky brightness temperature model is then derived, which includes contributions from the atmosphere and cosmic emissions at microwave frequencies. This model is used to calculate an approximation of the antenna noise temperature, when the antenna is pointed towards the sky and contributions from ground emission is ignored. Thereafter, the receiver noise temperature is defined as the effective noise temperature of the entire receiver system referenced to the antenna terminal. Contributions to the receiver noise temperature were discussed, where the noise from the first stage LNA is identified as the main contributor. The next chapter provides the design of a facility that is used to determine the system noise temperature of a receiver system.

Chapter 4

System Design

4.1 Introduction

This chapter discusses the design of a Hot-Cold antenna measurement system. Two known existing facilities are Temperature Hot And COld (THACO) test facility in the Netherlands and the Hot-Cold Test Facility (HCTF) in Canada. [2, 36] This chapter highlights the design considerations and limitations when developing such a system. Firstly, an investigation is given into the design of THACO at ASTRON [37], whereafter the design of a local system deployed at Stellenbosch University is discussed.

4.2 THACO - A Test Facility to Characterise Noise Performance of Antennas at ASTRON

Woestenburg [15] demonstrates that the system noise temperature of an antenna array can be derived from outdoor Y-factor measurements. The presented method creates a cold load by pointing the main antenna beam directly up toward the sky, while the hot load is created with absorbers. Though the measurements were successful at singular frequencies, it was noted that RFI and backside radiation obscure the accuracy of the results. A proposal was made to build a test facility that enables outdoor Y-factor measurements while minimizing RFI.

4.2.1 Principal Solution

Three solutions are proposed by ASTRON, to minimize the effects of RFI and backside radiation. These solutions are:

1. A facility that absorbs all backside radiation and uses a cooled cloche as the cold load and room temperature absorbers as the hot load.

2. A facility that reflects all backside radiation and uses the sky as the cold load and room temperature absorbers as the hot load.

3. An indoor freezing room that reaches low temperatures for cold measurements and room temperature for hot measurements.

Option 1 would have an adequate difference between the hot and cold measurement but using liquid nitrogen to cool the cloche for every measurement would be expensive. Option 3 would not provide a large enough difference between the hot and cold temperatures for a reliable measurement. Option 2 was seen as the best compromise between cost and reliability. The proposed concept design of the ASTRON test facility is shown in Figure 4.1, that is provided in [37].

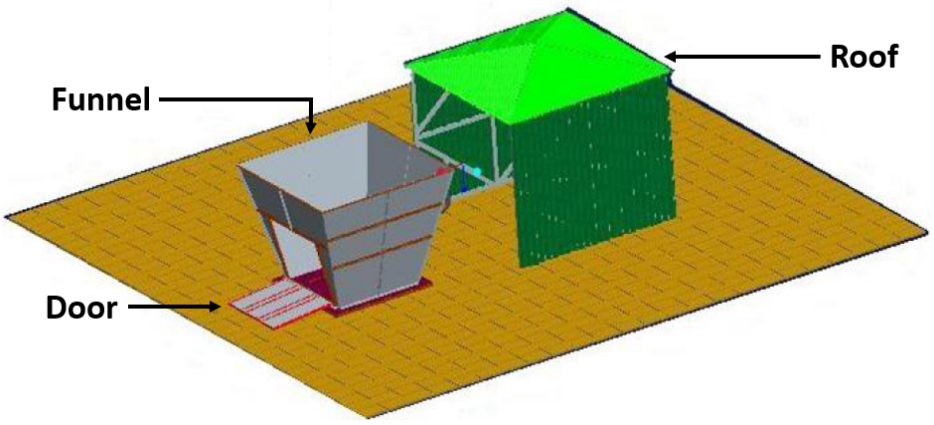

Figure 4.1: Proposed design of ASTRON outdoor Y-factor measurement facility.

The design of the funnel is constrained by frequency and size. The lower frequency limit for operation is 300 MHz, and the funnel should be large enough to fit an antenna array tile with enough space for someone to move inside. The starting point of the design is to choose a base size of the funnel that adheres to these above-mentioned constraints. The base is a $L \times L$ square area as shown in Figure 4.2. The parameters H and α are discussed later.

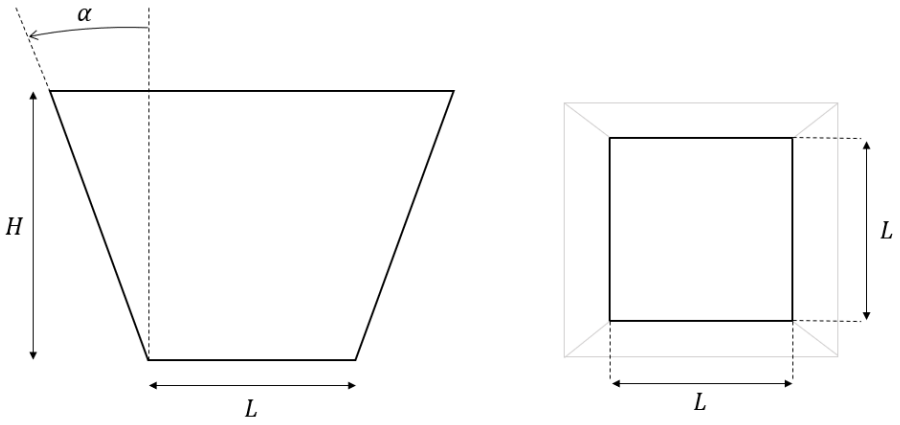

Figure 4.2: Illustration of the side view (left) and top view (right) of the funnel.

The minimum dimension for the base of the funnel is determined as follows. In terms of the frequency requirement, it is required that $L > \lambda_{\text{cut-off}}$, with the cut-off frequency $f_{\text{cut-off}} = 300$ MHz:

$$\lambda_{\text{cut-off}} = \frac{c}{f_{\text{cut-off}}} = \frac{3 \times 10^8}{300 \times 10^6} = 1 \text{ m}. \tag{4.1}$$

This means that L should thus be larger than 1 m to operate at the minimum frequency. In terms of the requirement to fit antennas inside the funnel, the maximum size of an antenna array tile developed at ASTRON is $1.5\,\text{m} \times 1.5\,\text{m}$. This means that L should be larger than 1.5 m. Taking both requirements into account $L > 1.5 \text{ m} > 1 \text{ m}$, the size of the base is thus chosen to be $2 \text{ m} \times 2 \text{ m}$. This leaves enough room for a person to enter the funnel while there is an antenna array tile inside.

4.2.2 Design Parameters and Simulation Setup

The funnel has an inverted truncated pyramid shape, as shown in Figure 4.1. The funnel is made of aluminium, which has non-ferrous properties and high conductivity, to shield electromagnetic interference. Aluminium is preferred for its high strength-to-weight ratio and low cost. [38]

The bottom size of the funnel, L, is chosen as 2 m to adhere to minimum frequency and space requirements. Figure 4.2 shows the design parameters of the funnel, where H is the height of the funnel and α is the flare angle of the walls.

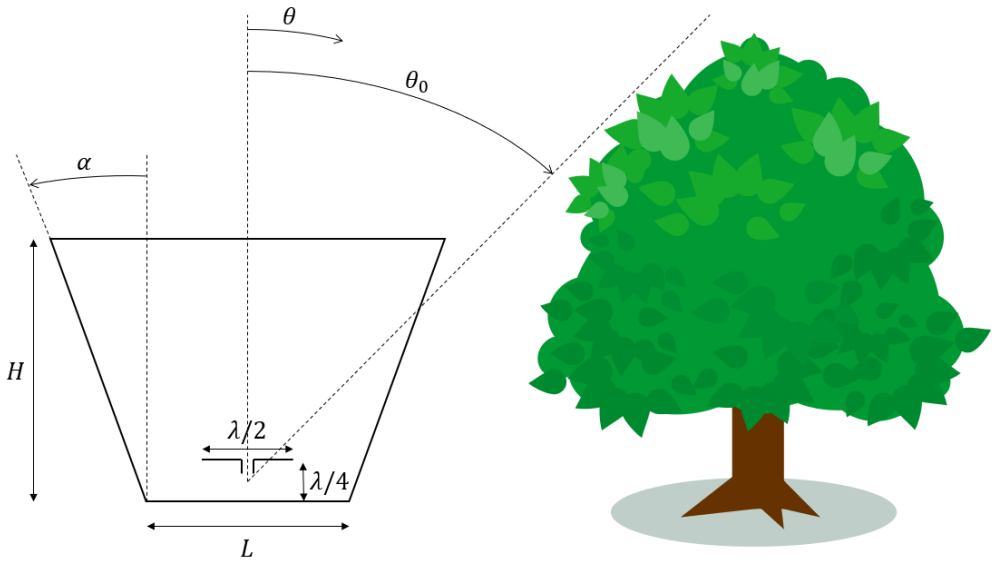

Figure 4.3: Funnel dimensions for simulation setup in environment.

The height H and angle α are determined by the minimum requirements for system noise temperature. For this design, the target specification is based on the system noise temperature requirements of the SKA. The target system noise temperature of the SKA is given as 30 K to 50 K. The measurement facility should not contribute more noise temperature than the target it should measure. An accuracy of at least 1/3 of the minimum noise temperature target is sufficient enough. Thus, the minimum system noise temperature contribution of the facility should be 10 K. [37]

A simulation is done to determine the noise temperature contribution of the funnel. This is completed by simulating a dipole antenna inside the funnel, as represented in Figure 4.3. The antenna noise temperature is calculated under the assumption of a specified temperature distribution in the environment outside the funnel. The assumed environment temperature distribution is specified as follows:

$$T_{\text{sky}} = 0 \text{ K} \qquad \text{for } 0° < \theta < \theta_0,$$

$$T_{\text{sky}} = 300 \text{ K} \qquad \text{for } \theta_0 < \theta < 180°,$$

where θ_0 is the angle at which environmental obstructions are seen by the antenna. Figure 4.3 uses the example of a tree as the environmental obstruction.

To find the preferred values for H and α, the far field of the dipole inside the funnel is simulated. The antenna noise temperature is calculated by using equation 3.3. The simulation is repeated by sweeping over different values of H and α at 300 MHz.

Table 4.1: Sweep parameters definition for THACO funnel simulation.

Parameter	Minimum value	Maximum value	Step size
H	2 m	3 m	0.1 m
α	0°	30°	5°

The results of the simulations are used to construct temperature plots for different θ_0 values. These plots are shown in Figure 4.4 and are used to identify the combinations of H and α where the noise temperature contribution of the funnel meets the target requirement.

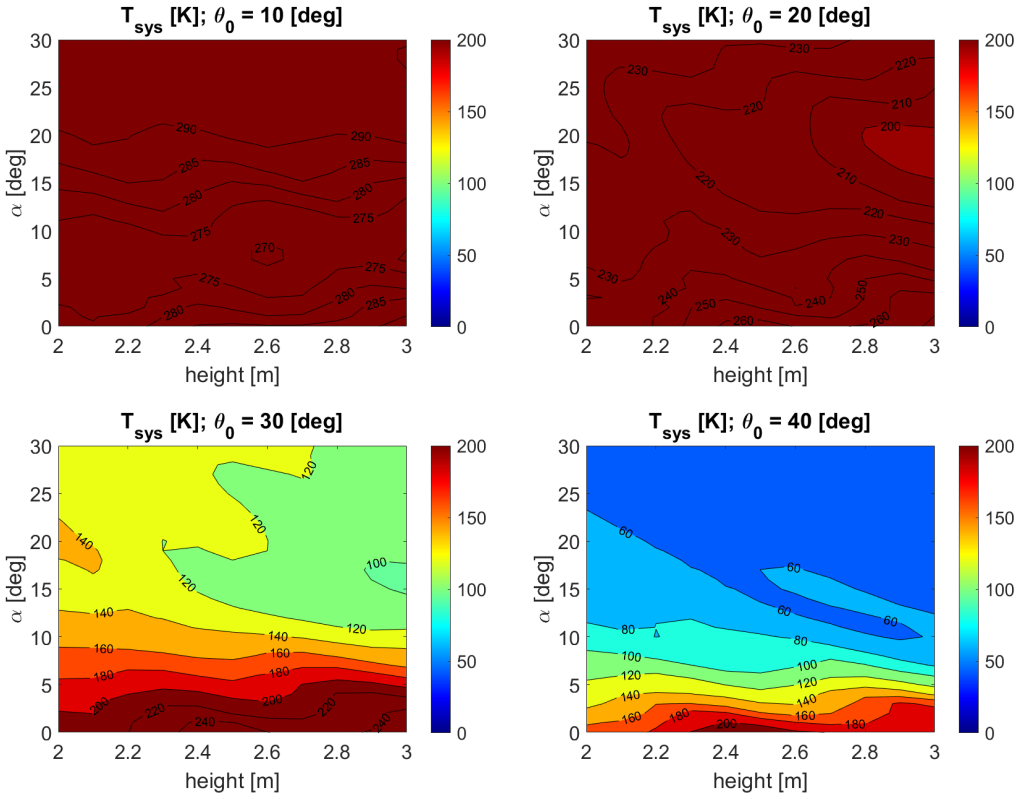

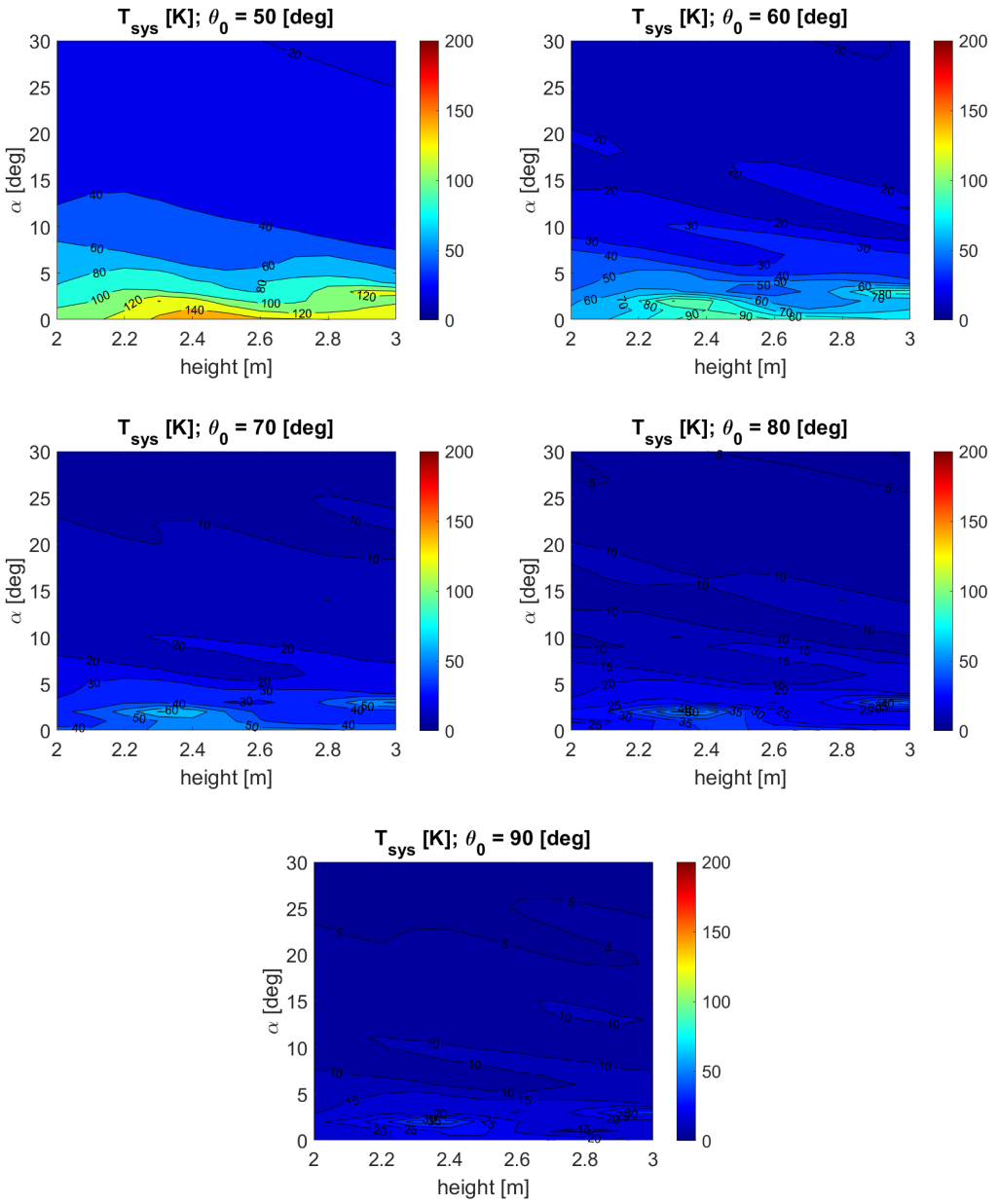

Figure 4.4: T_b for different dimensions of the funnel for different θ_0 values, with base length 2 m $\times$ 2 m.

The site is identified where THACO will be deployed and the nearest physical obstructions are investigated. The largest obstructions close to the site are the trees. The angle to the top of the trees is calculated to be about $\theta_0 = 80°$. Another large influence is the nearby Dwingeloo telescope. The angle to the top of the telescope is calculated as $\theta_0 = 75°$. This means that the size of the funnel can be chosen from the temperature plots for $\theta_0 = 70°$ and $\theta_0 = 80°$ from Figure 4.4.

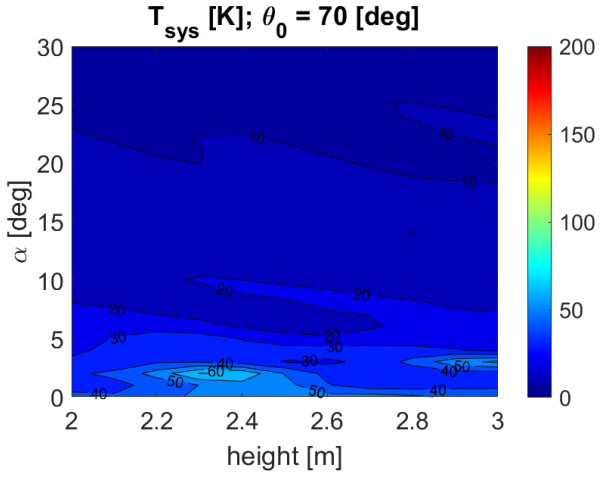

Figure 4.5: Temperature plot for $\theta_0 = 70°$

From Figure 4.5 the values of H and α can be derived where the antenna noise temperature is between 10 K and 20 K. With $H = 2.85$ m and $\alpha = 15°$ the antenna noise temperature is more or less 15 K. This satisfies the requirement for minimum noise temperature contribution by the funnel.

4.2.3 Design Summary

The design process of the outdoor Y-factor measurement facility is thus summarised as follows:

1. Identify the cut-off frequency, which determines the minimum size of the base, L.
2. Identify the measurement accuracy derived from the target specifications of the minimum system noise temperature.
3. Choose the site where the facility will be placed.
4. Identify possible environmental obstructions and calculate the θ_0 angle.
5. Choose the antenna noise temperature plot corresponding to the calculate θ_0 angle.
6. Verify that the antenna noise temperature is in the range of the required measurement accuracy and determine H and α.

Table 4.2: Designed parameters for THACO.

Parameter	Value
L	2 m
H	2.85 m
α	15°

Table 4.2 provides the designed parameters for the funnel structure of THACO. The roof of THACO is a movable carport, which can open to give the DUT a view of the cold sky, and close to view the ceiling that is filled with absorber material.

4.3 Design of SU-THACO

To design and build a Hot-Cold measurement system at Stellenbosch University requires considerations of inevitable factors. The university is situated in a busy town, which means the RFI activity is high. The environment is also densely populated with buildings and trees, so environmental obstruction is high. To deal with these factors, it is proposed to build the measurement system on the roof of the Electric and Electronic Engineering Department, shown in Figure 4.6. The name of the developed system is given as Stellenbosch University Temperature Hot And COld (SU-THACO) measurement system.

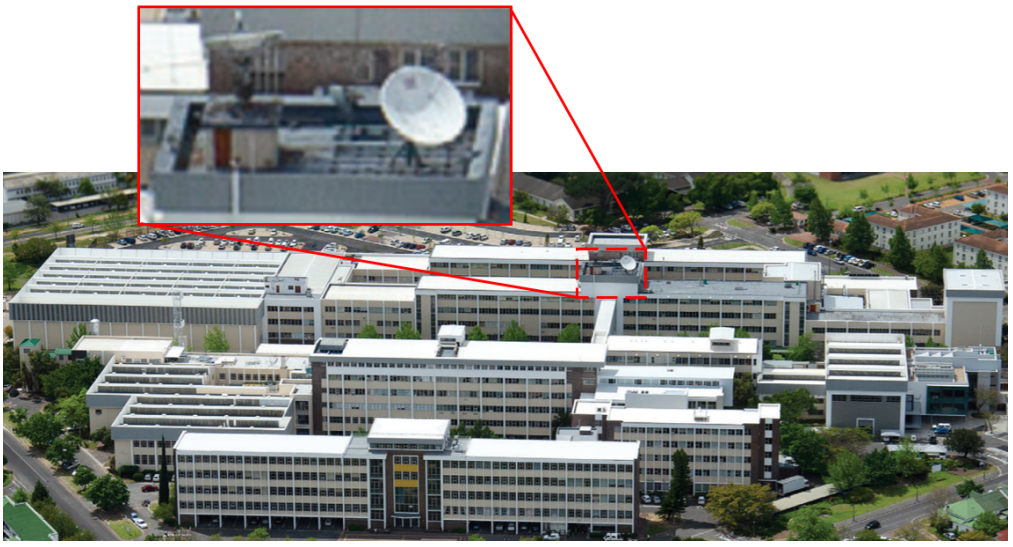

Figure 4.6: Proposed site to build SU-THACO.

The building is five stories high and there are not many physical obstructions nearby, which decreases the amount of environmental obstruction in the antenna field of view. The RFI activity is also investigated between 300 MHz

and 2 GHz, which includes the MFAA band, to identify frequency bands where reliable measurements can be made.

4.3.1 Investigation of Site

The first step taken before designing the local Hot-Cold measurement system is to investigate the available site in terms of obstructions and RFI. Measuring the RFI in the environment helps to identify the cut-off frequency for the system. Identifying physical obstructions close to the site helps to determine θ_0.

4.3.1.1 Measuring the RFI

To do a Y-factor measurement, it is important to have a distinguishable difference between the hot and cold measurement. This becomes difficult when the hot and cold measurement is done in an RFI-rich environment. A high noise floor and unwanted peaks in the measurement makes the detection of small power changes difficult, which is necessary for a Y-factor calculation.

An RFI measurement is taken by measuring the signal strength in the environment using a spectrum analyser. A Log Periodic Dipole Antenna (LPDA) and a Rohde and Schwarz FSEK30 spectrum analyser are used to perform the measurement. The measurement is taken from 300 MHz to 2 GHz, with the spectrum analyser set to hold the maximum value of the measured power level over time. The result is shown in Figure 4.7.

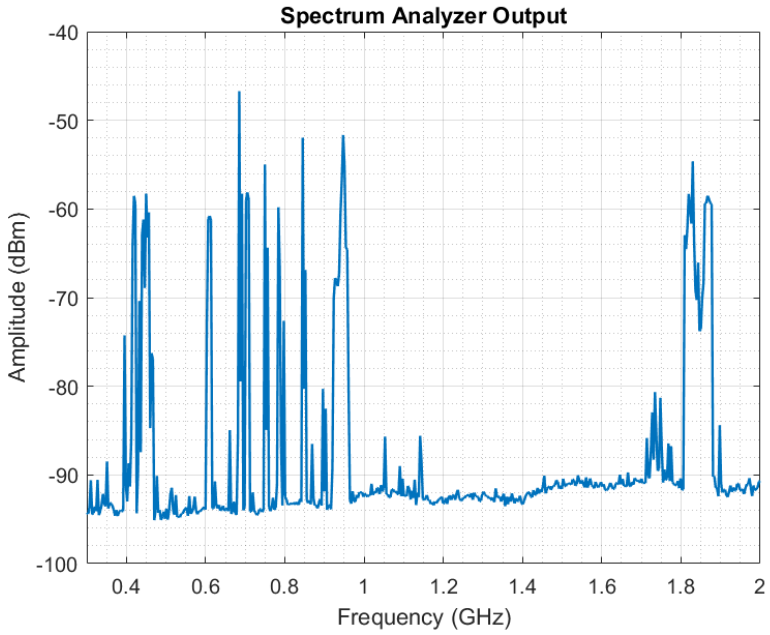

Figure 4.7: Measured RFI on the roof of the Electric and Electronic building at Stellenbosch University.

From Figure 4.7 it is observed that there are various sources of RFI activity below 1 GHz and a prominent peak at 1.8 GHz. The peaks at 900 MHz and 1.8 GHz are attributed to the Global System for Mobile communication (GSM), which are also the frequencies that cell phone towers operate at. The peaks between 470 MHz and 854 MHz are attributed to UHF-television signals. [39]

Apart from the peak at 1.8 GHz, the RFI density from 1 GHz to 2 GHz looks comparatively lower. Therefore, the cut-off frequency for SU-THACO is chosen as

$$f_{\text{cut-off}} = 1 \text{ GHz}. \tag{4.2}$$

The frequency range for the measurement system is chosen as 1 GHz to 2 GHz.

4.3.1.2 Identifying possible obstructions

For the cold measurement, it is preferred to have a clear view of the sky. This means that there should preferably not be physical obstructions surrounding the measurement system.

At the proposed site for SU-THACO, there is a large antenna that might pose as an obstruction. A range finder is used to measure the distance from the SU-THACO site to the top of the antenna.

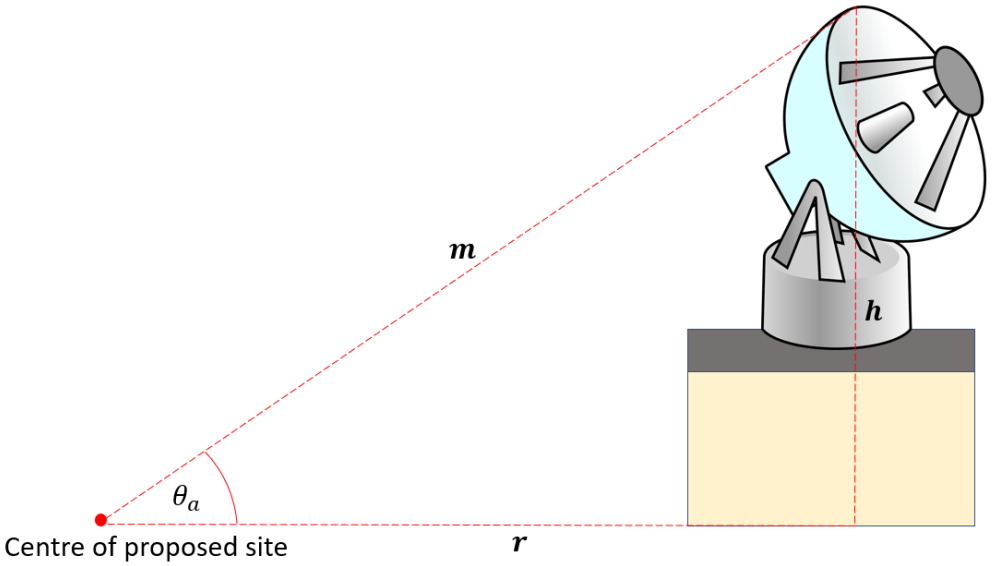

Figure 4.8: Graphical representation of physical obstruction identified near SU-THACO site.

Figure 4.8 shows how the angle θ_a is found. The variable m represents the hypotenuse, h the opposite side and r the adjacent side. The distance to the

highest point of the antenna is measured as:

$$m = 12.48 \text{ m} \tag{4.3}$$
$$h \approx 6 \text{ m}. \tag{4.4}$$

Thus, θ_a is calculated as,

$$\theta_a = \sin^{-1}\left(\frac{h}{m}\right) = 28.74°. \tag{4.5}$$

As θ_0 is the angle measured from zenith, it is determined as,

$$\theta_0 = 90° - \theta_a = 61.26°. \tag{4.6}$$

This calculation means that for approximately 60° from zenith, the device under test has a clear view of the sky.

4.3.2 Simulations for SU-THACO

The parameters H and α of the funnel are determined through simulation. Temperature plots are generated and used to identify the parameter values where the noise temperature contribution of the system is within the required measurement accuracy. The measurement accuracy for SU-THACO is also based on the requirements for the system noise temperature of the SKA. The minimum noise contribution of the system should thus be between 10 K and 20 K.

The chosen cut-off frequency for SU-THACO is 1 GHz. The minimum size of the base at operating frequency is determined as:

$$\lambda_{\text{cut-off}} = \frac{c}{f_{\text{cut-off}}} = \frac{3 \times 10^8}{1 \times 10^9} = 0.3 \text{ m}. \tag{4.7}$$

This means that $L > 0.3$ m, to adhere to frequency requirements of SU-THACO. A base of 0.3 m is quite small to fit an antenna array in the measurement system. To accommodate for antenna arrays, the base size of SU-THACO is thus chosen as

$$L = 1 \text{ m}. \tag{4.8}$$

The temperature plots are generated by simulating a dipole antenna inside the funnel structure, as seen in Figure 4.3. A parameter sweep is done for different values of H and α. The sweep parameters are defined in Table 4.3.

Table 4.3: Sweep parameters definition for SU-THACO funnel simulation.

Parameter	Minimum value	Maximum value	Step size
H	1 m	2 m	0.1 m
α	0°	30°	5°

The generated far-fields are used in equation 3.3 to calculate the antenna temperature for different θ_0 values. The simulated plots are shown in Figure 4.9 below.

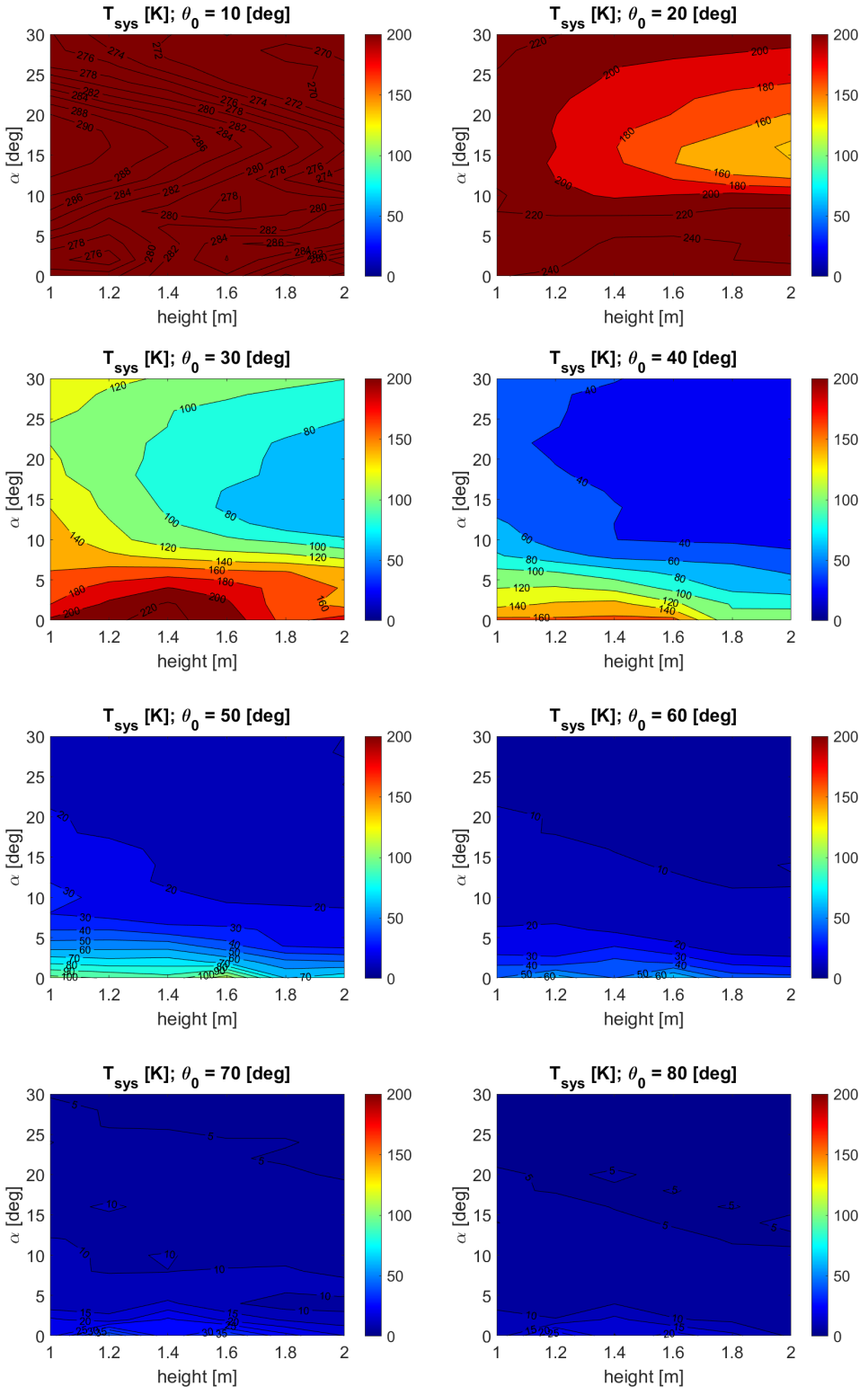

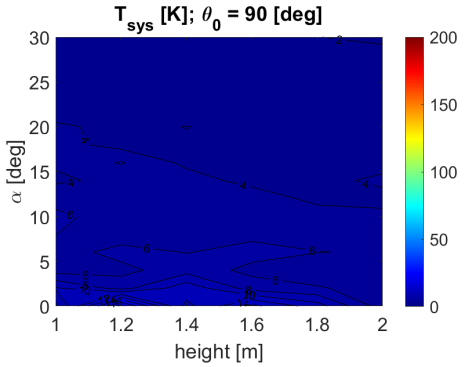

Figure 4.9: T_b for different dimensions of the funnel for different θ_0 values, with base length 1 m $\times$ 1 m.

The measured θ_0 value at the site of SU-THACO is 61.26°, as given in equation 4.6. The temperature plot for $\theta_0 = 60°$ is thus used to chose the H and α values for SU-THACO.

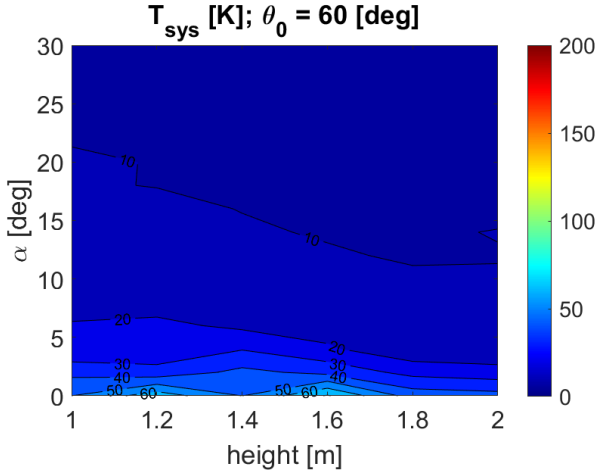

Figure 4.10: Temperature plot for $\theta_0 = 60°$ of SU-THACO.

From Figure 4.10 it is observed that the antenna noise temperature for all H values at the α angle larger than 10°, is in the required measurement accuracy of 10 K. This allows the final values of H and α to be chosen in satisfaction with other physical constraints.

4.3.3 Physical Design of SU-THACO

To finalise the design of the measurement system, important factors have to be considered. Firstly, the structure consists of three integral parts: the funnel, the roof covered with absorber material and a door to access the inside of the funnel. Secondly, the roof has to be a removable structure to change between

the hot and cold states. Finally, the structure should be manufacturable inside the Electric and Electronic workshop of Stellenbosch University and be movable to the roof. Doors are typically 2 m high, so the maximum height of any section should not exceed this restriction.

The material chosen for the SU-THACO facility is 2 mm aluminium, for its weight, cost and non-ferrous properties. The skin depth of aluminium is 0.0033 mm at 1 GHz. [25, Ch. 6, pp. 245-248]. This indicates that a 2 mm aluminium facility will provide a sufficient shield between 1 GHz and 2 GHz.

4.3.3.1 Roof

The absorber material available at Stellenbosch University is 8 inch Eccosorb VHP, from Emerson and Cuming Anechoic Chambers. [40]

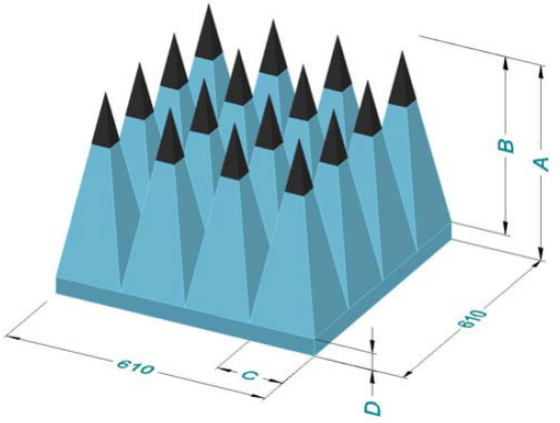

Figure 4.11: Absorber material size definition.

Each block of the absorber material is 610 mm by 610 mm. The dimensions of the parameters in Figure 4.11 are provided in Table 4.4, for the 8 inch Eccosorb VHP.

Table 4.4: Parameter dimensions of absorber material blocks.

	A	**B**	**C**	**D**
Dimension (mm)	203	178	68	25

If the blocks are placed in a 3×3 square, it is 1 830 mm in length and width. Thus the roof is chosen to be 1 900 mm by 1 900 mm, so that a 3×3 square of absorber material can be placed on it and can still fit through a door.

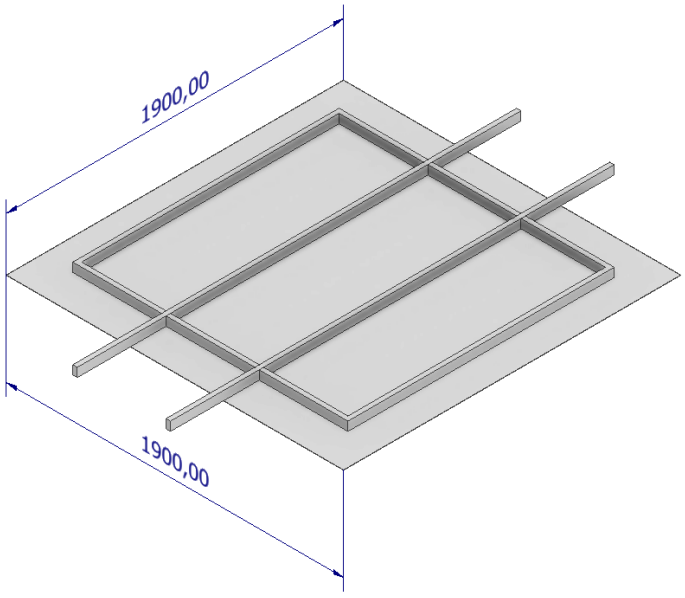

Figure 4.12: Drawing of the roof with its support structure and handles.

For stability, 25 mm by 25 mm 2 mm rectangular aluminium tubing is attached to the top of the roof, to make it easier to handle. A drawing of the top of the roof, illustrating the handles are shown in Figure 4.12.

4.3.3.2 Funnel

In a personal interview, Dr. Rob Maaskant, who worked on the original simulations of THACO, highlighted that care should be given to seams on the walls and door of the structure. This was again mentioned in an interview with Dr. David Prinsloo, who is employed by ASTRON and has worked with THACO, as he explained that the seams on the walls have a noticeable influence when measuring receiver systems with broad beamwidths.

To minimize seams in the funnel structure, it is chosen to have each wall section cut from an individual aluminium sheet. Standard aluminium sheets are 1 250 mm by 2 500 mm.

Two pre-determined dimensions for the funnel is the base size of 1 000 m and the size of the top opening to fit the roof. The absorber material has similar physical properties to a sponge, which means they can deform to fit into tight spaces. Thus the top opening of the funnel is chosen to be 1 800 mm so that the absorber material can fill the space.

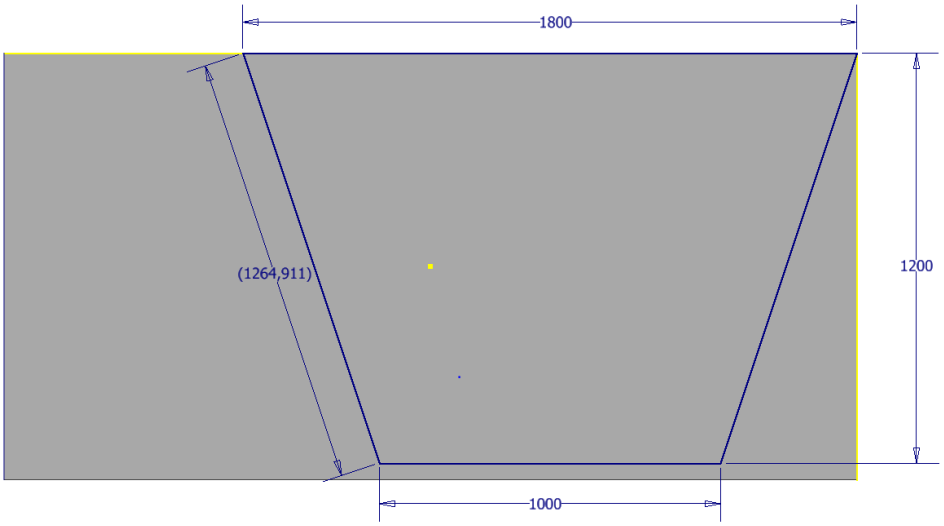

Figure 4.13: Demonstration of the wall sections cut from a single aluminium sheet.

If the height of each wall section is chosen as 1.2 m, it is possible to cut a section from a single aluminium sheet. Thus accordingly, the H value of the funnel is 1.13 m and the α value 20°. The designed parameters are shown in Table 4.5.

Table 4.5: Designed parameters for SU-THACO.

Parameter	Value
L	1 m
H	1.13 m
α	20°

4.3.3.3 Skeleton frame

Now that the dimensions of the structure are determined, a design choice is made on how the structure is going to be assembled and supported. Firstly, to aid this decision a simulation is done to determine the currents that are excited on the surface of the structure.

A simulation is done in FEKO, where a dipole antenna is simulated inside the funnel of SU-THACO. The funnel has the height of 1.13 m, flare angle of 20°, bottom width of 1 m and top width of 1.8 m. The funnel is constructed with 2 mm aluminium.

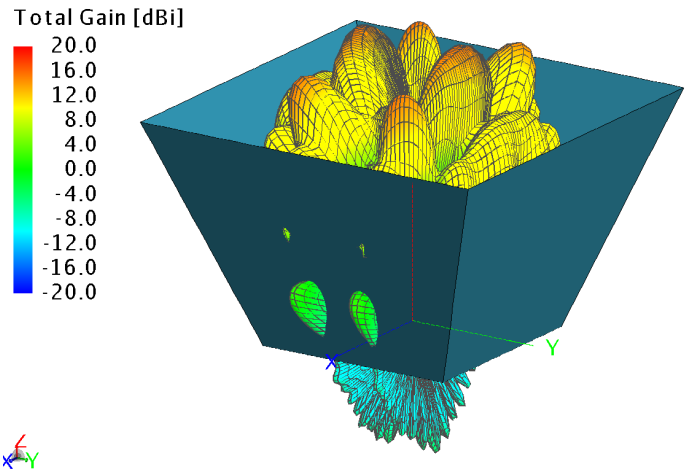

Figure 4.14: Simulated far-field of dipole antenna inside SU-THACO.

Figure 4.14 shows the simulated far-field of the dipole antenna inside the funnel at 1 GHz. Figure 4.15 and Figure 4.16 shows the cartesian plots of the radiation pattern.

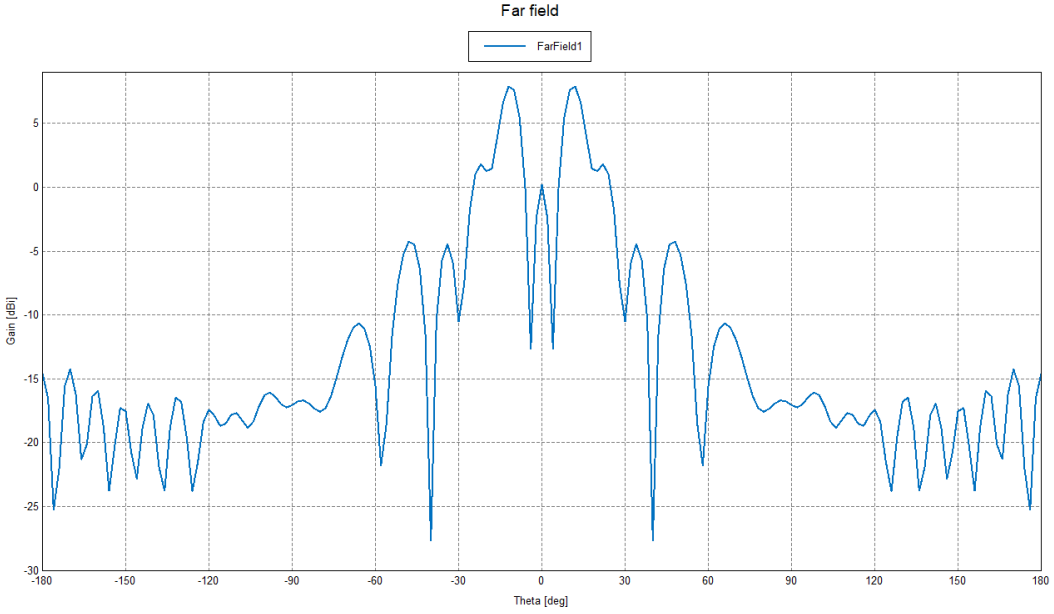

Figure 4.15: Far-field radiation plot, $\phi = 0°$

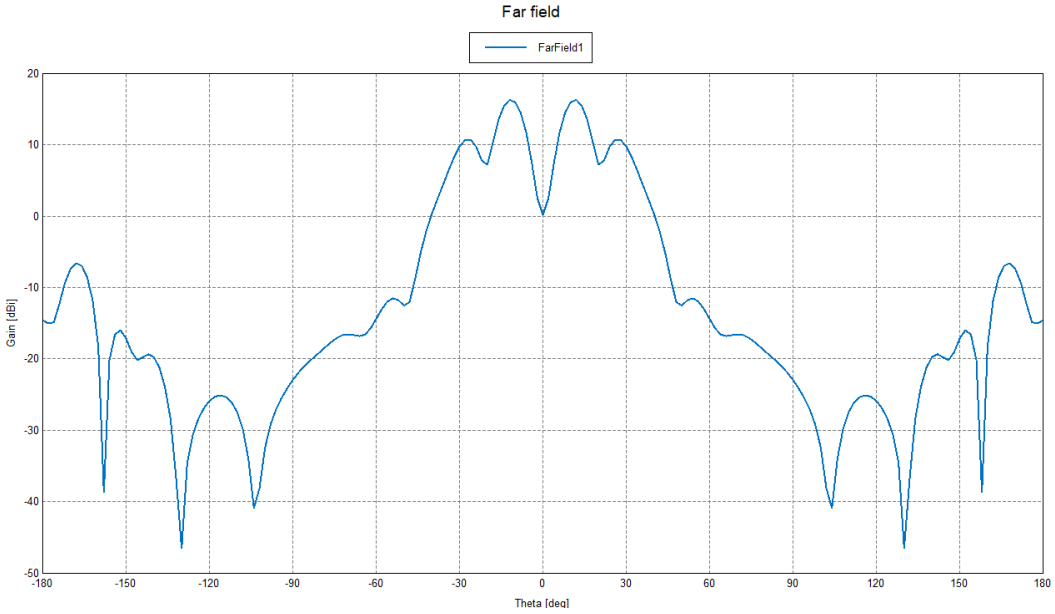

Figure 4.16: Far-field radiation plot, $\phi = 90°$

The surface current is simulated and the result is shown in Figure 4.17.

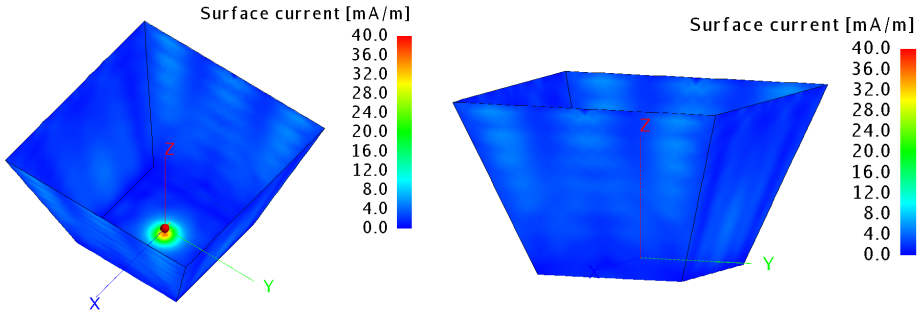

(a) View of excited dipole inside.

(b) Side view of outside walls.

Figure 4.17: Simulated surface currents on SU-THACO with a 1 V port excitation dipole at 1 GHz.

From Figure 4.17 it is observed that minimal currents are excited in the corners of the funnel. This inspires the idea to design a skeleton frame that will support SU-THACO and allow for simpler assembly of the structure.

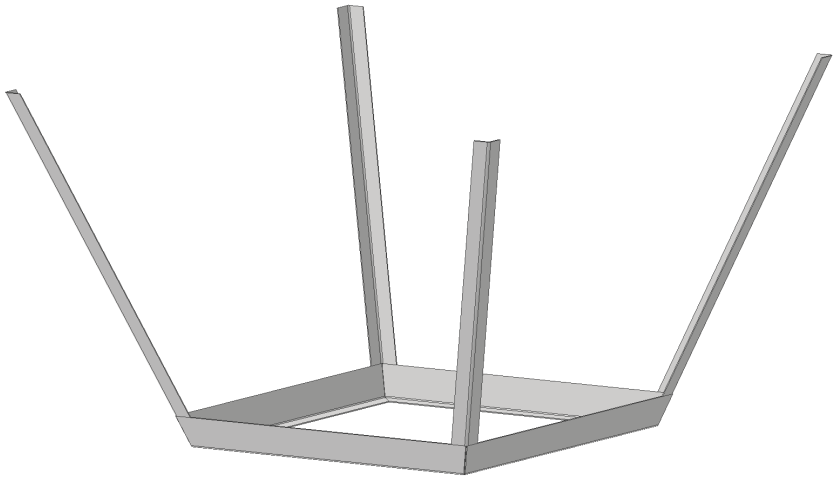

Figure 4.18: Skeleton frame for support and construction of SU-THACO.

The frame is designed so that the wall sections can be attached to it. Figure 4.18 shows the designed skeleton frame and Figure 4.19 below, shows how the walls are attached to the frame. A small space is given at the top of the funnel, as can be observed in Figure 4.19, to give more room for the absorber material to fit into.

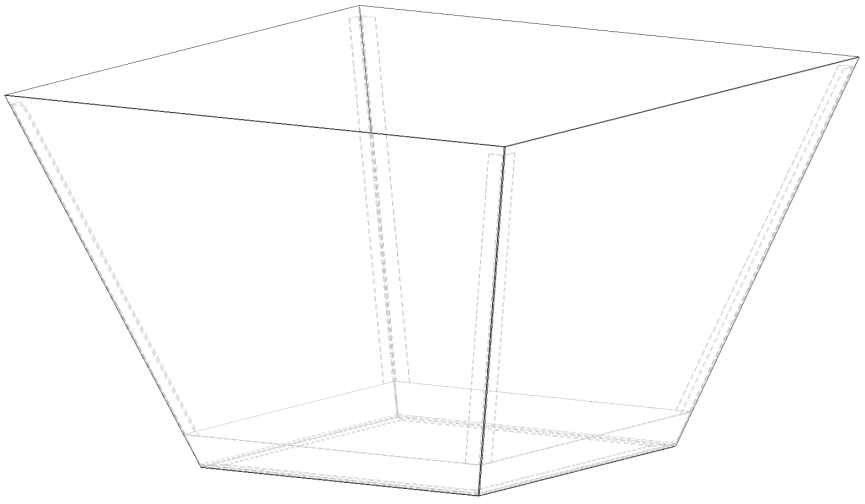

Figure 4.19: A view of the frame inside SU-THACO.

4.3.3.4 Door

For simplicity, the door is chosen to be a wall section that can reattach with clamps. The wall section used for the door is supported with 25 mm by 50 mm 3 mm rectangular aluminium tubing, as shown in Figure 4.20. The added aluminium tubing provides stability and enough room to make the door easy to handle.

To ensure that the door makes electrical contact with the frame section, Beryllium-Copper finger-strips are added to the edge of the door. [41] These finger-strips compresses to provide electrical contact between the two metal surfaces and shields currents from entering through any gaps left between the door and frame. Rubber sealing strips are also placed on the outer edge of the door. [42] The rubber strips have shielding properties, but their main purpose is to protect the Beryllium-Copper finger-strips from being compressed to their maximum.

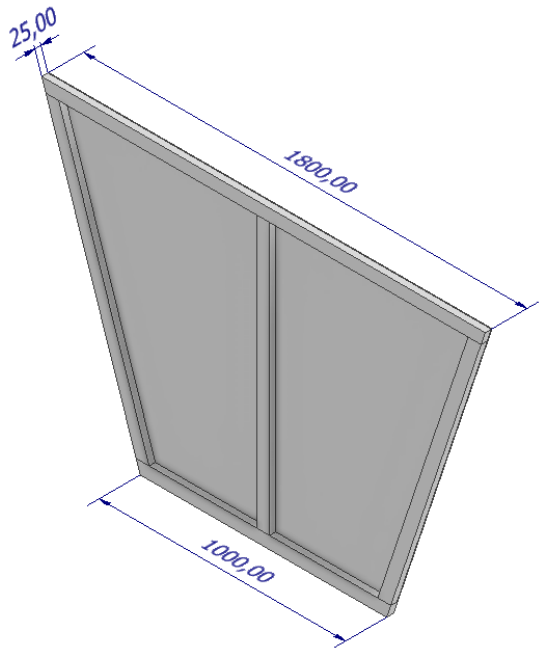

Figure 4.20: Drawing of the door with its support structure.

4.3.4 Back-end Design of SU-THACO

The back-end of SU-THACO consists of a spectrum analyser and a laptop that runs a MATLAB GUI. A diagram representing the back-end of SU-THACO is shown in Figure 4.21, which also indicates how the different systems are connected.

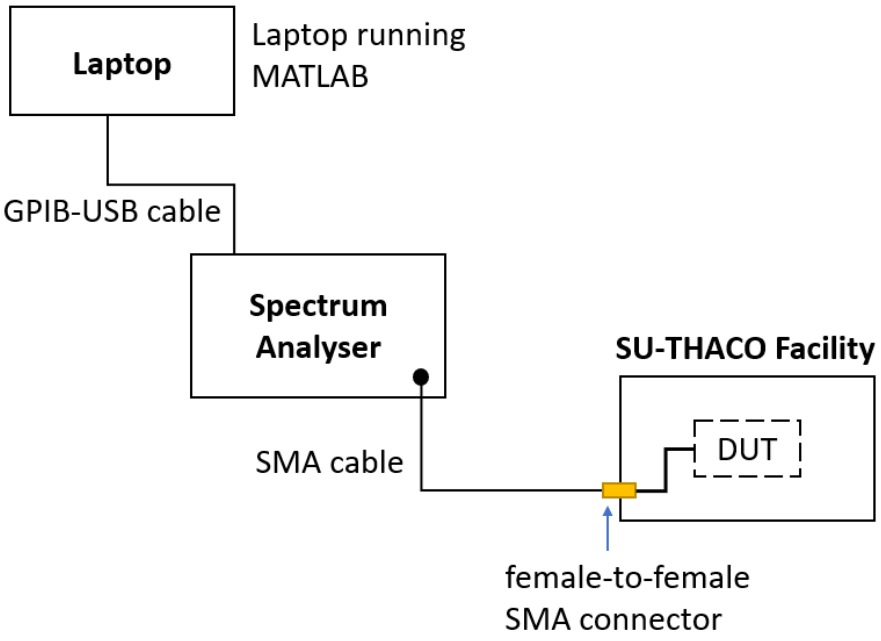

Figure 4.21: Diagram representing the back-end of SU-THACO system.

4.3.4.1 Connections and Cabling

A female-to-female SMA connector and an SMA cable are used to connect the DUT inside the SU-THACO facility to the spectrum analyser. The SMA cable used for this connection should have minimal attenuation, to not obscure information measured from the DUT. A catalogue is established of the available cables for the measurement system, and their attenuation at 2 GHz is given in Table 4.6.

Table 4.6: Catalogue of available SMA cables at Stellenbosch Electric and Electronic Engineering Microwave laboratory.

Name	Manufacturer	Attenuation at 2 GHz [dB/m]	Opperating frequency [GHz]
SPUMA_400	HUBER+SUHNER	0.19	6
EZ_141_AL	HUBER+SUHNER	0.57	33
EZ_141_CU	HUBER+SUHNER	0.54	33
MULTIFLEX_141	HUBER+SUHNER	0.58	33
SUCOFLEX_104	HUBER+SUHNER	0.34	26.5
LMR-100A	Times Microwave Systems	1.15	5.8
LMR-195	Times Microwave Systems	0.55	5.8
LMR-240	Times Microwave Systems	0.38	5.8
LMR-400	Times Microwave Systems	0.19	5.8

From the available cables, a 50 cm LMR-240 cable and a 1 m LMR-400 cable are the best options. The LMR-400 cable is preferred for its length, minimal attenuation and outdoor capabilities. LMR-400 cables are designed for outdoor exposure, which incorporates materials for UV protection and provides RF shielding rated at $>$ 90 dB. [43] A hole is drilled through one of the walls of the SU-THACO facility, where an Ampenol panel mount connector is used to provide a connection between the inside and outside of the facility. The connector has an impedance of 50 Ω and operates from DC to 18 GHz. [44] The connection between the spectrum analyser and the laptop is provided with a GPIB-USB cable.

4.3.4.2 GUI for SU-THACO

A MATLAB GUI runs on the laptop, which communicates with the spectrum analyser. It has basic functionality, which is to save measurements in a folder, prompt the user to place or remove the roof from the structure for the hot or cold measurement and provide an initial Y-factor calculation.

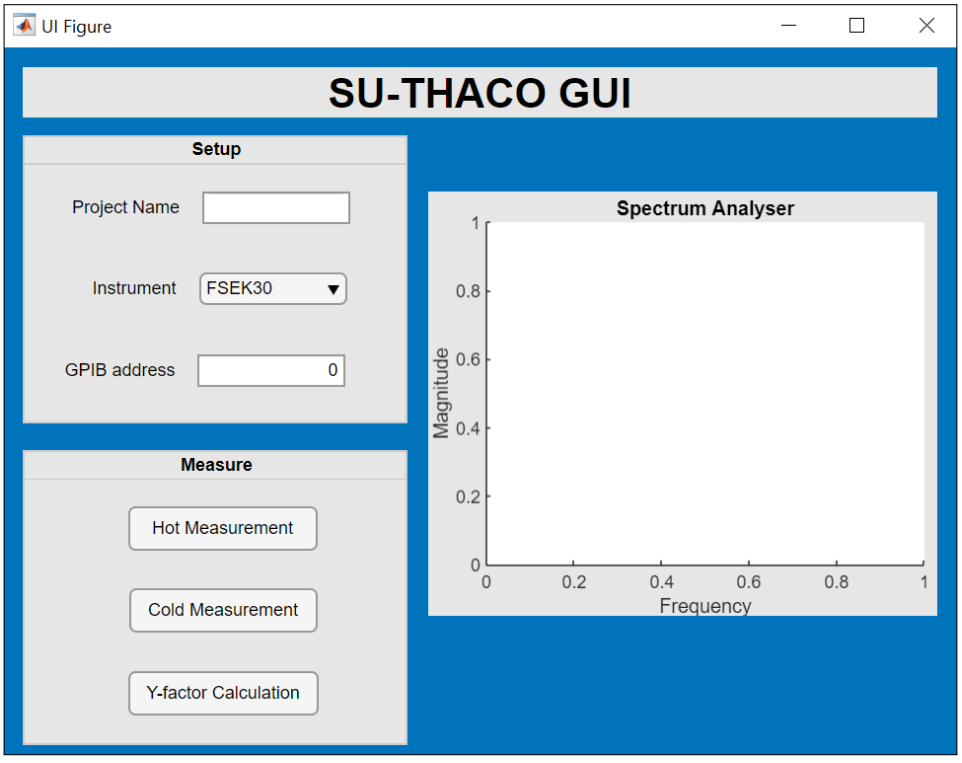

Figure 4.22: SU-THACO GUI.

The SU-THACO GUI, shown in Figure 4.22, includes a setup and measure field, and a plot to view the measured results. A description of the use of the SU-THACO GUI is given in Appendix A.

4.4 Manufacturing

The manufacturing is done at the Electric and Electronic Engineering workshop of Stellenbosch University. The funnel is assembled by first placing the frame sections and thereafter the surrounding walls. Holes are drilled before moving the structure to the roof. The box is positioned on the roof and the walls are attached with rivets to the frame structure. The clamps for the door are fixed on opposite sides of the funnel structure. Figure 4.23 shows the completed facility on the roof.

Figure 4.23: The assembled measurement facility on the roof of the Engineering Faculty of Stellenbosch University.

4.5 Conclusion

The design of a Hot-Cold measurement system to be deployed on the roof of the Electric and Electronic Engineering building of Stellenbosch University, is discussed in this chapter. After a study on the designed measurement system at ASTRON, similar steps are followed to design the local measurement system. An investigation of the RFI at the site for the local measurement system, identified the frequency range of 1 GHz to 2 GHz to be chosen as the initial operating frequency of the local Hot-Cold measurement system. The facility is shaped like a truncated pyramid, with a height of 1.13 m, flare angle of

20°, bottom width of 1 m and top width of 1.8 m. A skeleton frame was designed to support the structure, which is build from 2 mm aluminium. The fabricated measurement system, named SU-THACO, is deployed on the roof and measurements are presented in the following chapter.

Chapter 5

Results

5.1 Introduction

This chapter gives an overview of the results from the developed Hot-Cold measurement system at Stellenbosch University. Firstly, the level of RFI suppression inside the facility is investigated. Secondly, a review of calibration for the measurement system is given, where the noise temperature of the measurement setup is calculated. Thereafter, measured results are shown of an active antenna, to indicate the accuracy achieved with SU-THACO. Measurements are done with a Rohde and Schwarz FSEK30 spectrum analyser [45] and the typical setup is shown in Figure 5.1 with the door open. The SU-THACO GUI is used to do the Y-factor measurements in this chapter.

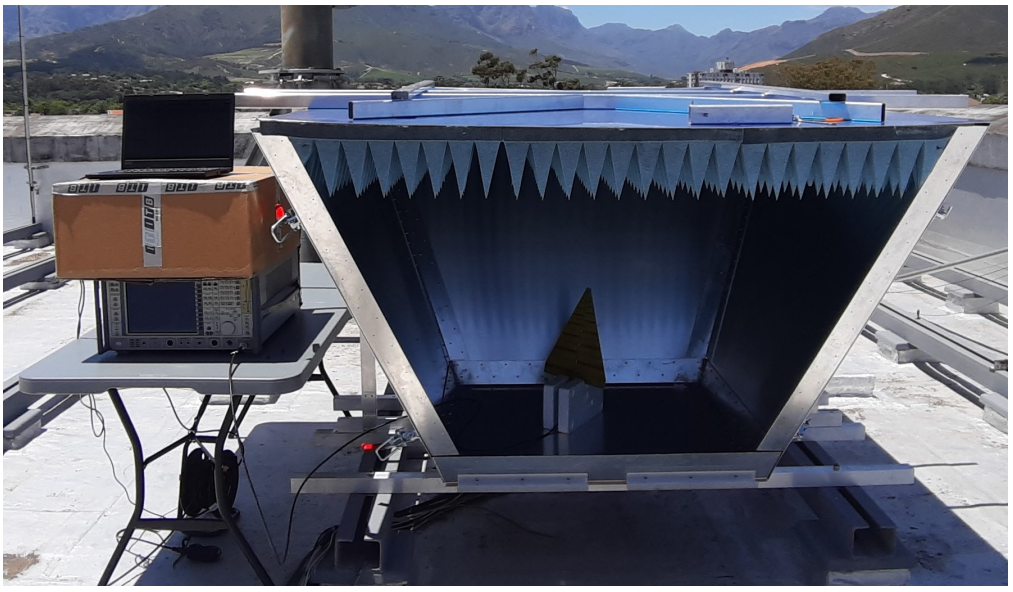

Figure 5.1: Typical measurement setup for doing measurements inside SU-THACO.

5.2 RFI Suppression

The main purpose of the measurement system is to minimize the RFI when doing an outdoor Y-factor measurement. The level of suppression inside the measurement system is investigated by measuring the RFI outside and inside the measurement system. An LPDA is used to do the measurement from 0.5 GHz to 2 GHz.

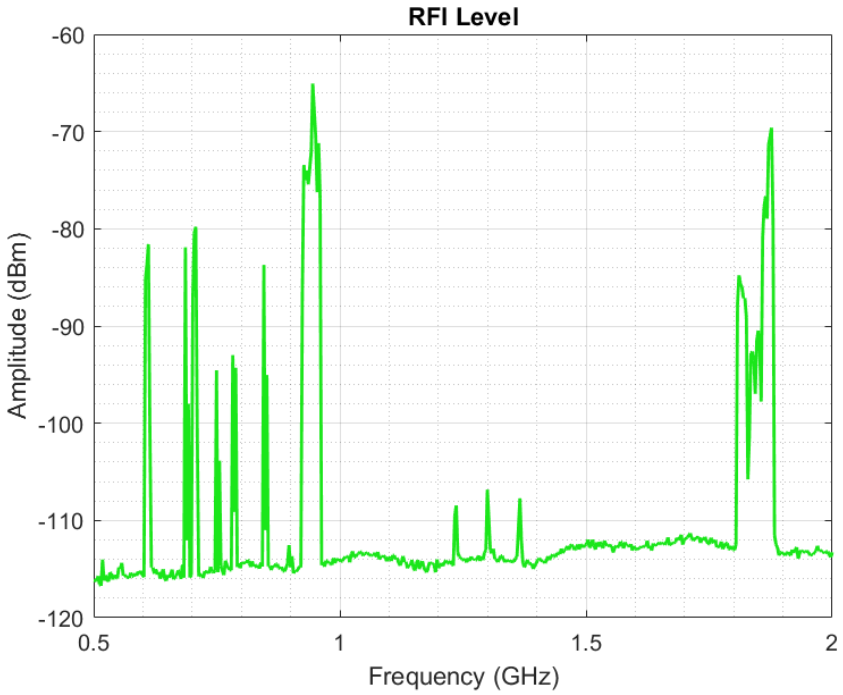

Figure 5.2: Plot of measured RFI level in the environment outside SU-THACO.

Figure 5.2 shows the RFI level measured outside the measurement facility. In the frequency band for SU-THACO, 1 GHz to 2 GHz, it is observed that there are three peaks between 1.2 GHz and 1.4 GHz, and a larger peak spanning from 1.8 GHz to 1.9 GHz.

The three peaks between 1.2 GHz and 1.4 GHz, are attributed to radio-navigation and satellite communication. [46] They are measured as -108.5 dBm at 1.236 GHz, -106.8 dBm at 1.3 GHz and -107.7 dBm at 1.366 GHz. The peak spanning from 1.8 GHz to 1.9 GHz, is attributed to GSM. The peak is measured as -84.78 dBm at 1.81 GHz and -69.61 dBm at 1.88 GHz.

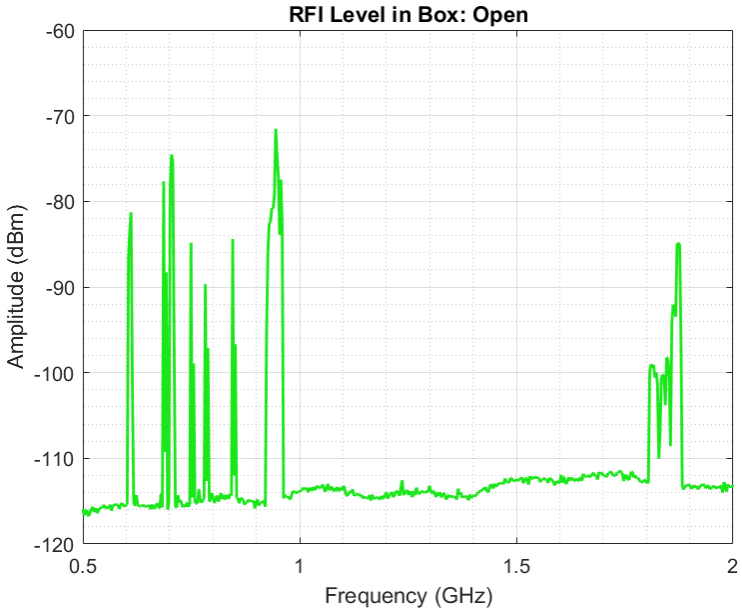

Figure 5.3: Plot of measured RFI level inside SU-THACO with the roof opened.

Figure 5.3 shows the RFI measurement inside SU-THACO with the roof opened. Comparing this result to Figure 5.2 over the band of interest, it is clear that the three peaks between 1.2 GHz and 1.4 GHz are not observed. A measurement at 1.3 GHz. The peaks are suppressed by 6.4 dBm to the noise floor level of the spectrum analyser. The peak between 1.8 GHz and 1.9 GHz is still present, but was suppressed by 15.19 dBm at 1.81 GHz and 15.34 dBm at 1.88 GHz.

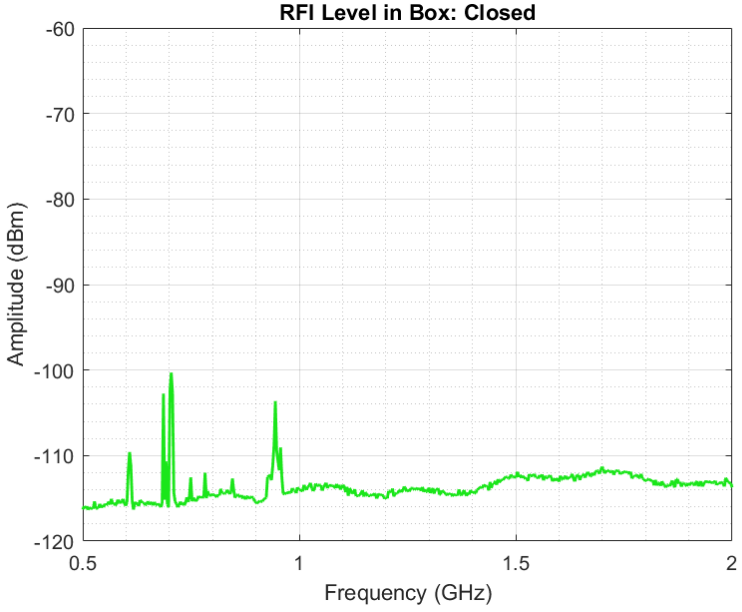

Figure 5.4: Plot of measured RFI level inside SU-THACO with the roof closed.

Figure 5.4 shows the RFI measurement inside SU-THACO with the roof closed. It is observed that the RFI over the band of interest, 1 GHz to 2 GHz, is suppressed to the noise floor level of −113 dBm. The largest peak at 1.88 GHz is suppressed by 43.39 dBm, which indicates the level of suppression achieved when the roof is closed. The small peaks that are present below 1 GHz are not of interest, as it falls below the cut-off frequency of the measurement system.

The RFI measurements shows promising results over the band of interest, but caution should be given to RFI influence between 1.8 GHz and 1.9 GHz, as the RFI is not fully suppressed for the open-roof measurements.

5.3 Calibration Step

In accordance with Friis's formula, as given by equation 2.25, the measured output power would be a function of the DUT and contributions from the measurement setup. The total noise temperature, T_{TOT}, is expressed as

$$T_{\mathrm{TOT}} = T_{\mathrm{DUT}} + \frac{T_{\mathrm{SPEC}}}{G_{\mathrm{DUT}}}, \tag{5.1}$$

where T_{DUT} is the noise temperature of the DUT, G_{DUT} the gain of the DUT, and T_{SPEC} the noise temperature contribution of the measurement setup. The noise temperature of the DUT is then calculated as,

$$T_{\mathrm{DUT}} = T_{\mathrm{TOT}} - \frac{T_{\mathrm{SPEC}}}{G_{\mathrm{DUT}}}. \tag{5.2}$$

Thus, the noise temperature of the measurement setup and the gain of the DUT should be known before doing the measurement.

The noise temperature of the measurement setup, T_{SPEC}, includes the noise temperature contribution from the spectrum analyser, the pre-amplifier and the cables. A pre-amplifier is included for improved measurement sensitivity. [47] To determine T_{SPEC}, a Keysight 346B noise source [48] is used to do a Y-factor measurement. The noise source has an ENR of 15.4 dB between 1 GHz and 2 GHz. The noise source is connected to the measuring setup and switched between on and off for the hot and cold measurements. The measurements are done at the centre frequency of 1.575 GHz and a bandwidth of 50 MHz, which is the same frequency range where T_{DUT} is measured.

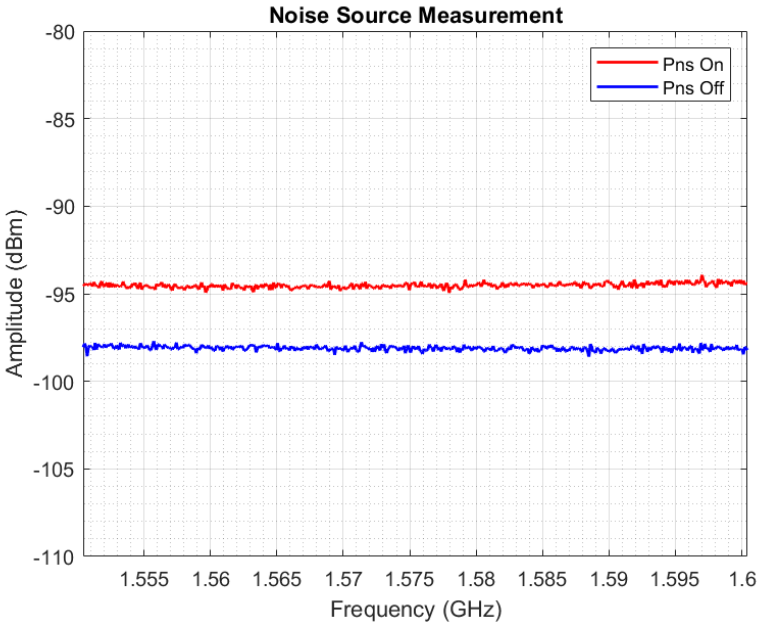

Figure 5.5: Hot and cold measurement of T_{SPEC}.

Figure 5.5 clearly shows a difference when switching the noise source on and off. The average power level measured while the noise source is switched on is -94.52 dBm, and -98.11 dBm when the noise source is switched off. The data is used to calculate the Y-factor value of the measurement, which is shown in Figure 5.6. The calculated Y-factor value averages around 2.288.

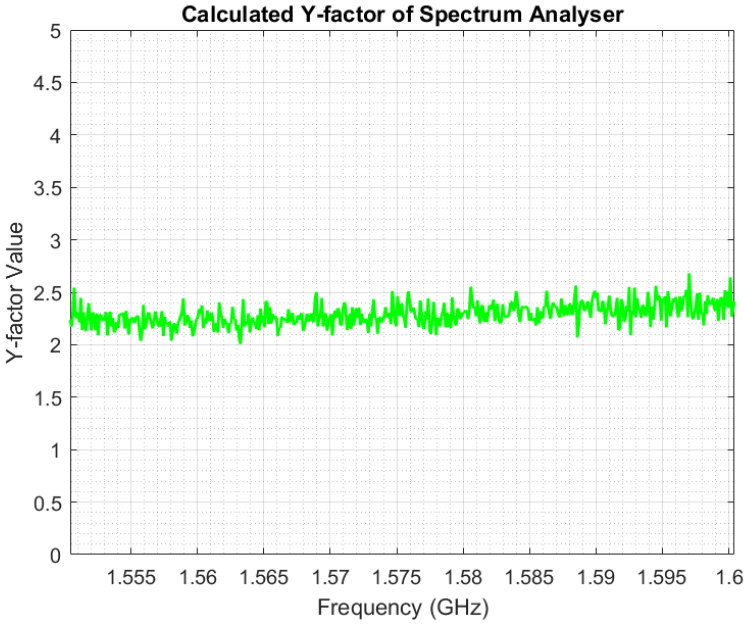

Figure 5.6: Calculated Y-factor value of T_{SPEC} measurement.

After the Y-factor value is calculated, the noise temperature of the measurement system can be calculated as:

$$T_{\text{SPEC}} = \frac{T^{\text{on}} - Y_{\text{SPEC}} T^{\text{off}}}{Y_{\text{SPEC}} - 1}, \tag{5.3}$$

where $T^{\text{off}} = 290$ K is the reference noise temperature when the noise source is switched off, and T^{on} is the reference noise temperature when the noise source is switched on, which is calculated as:

$$T^{\text{on}} = 290\left(1 + 10^{(15.4/10)}\right) \tag{5.4}$$

$$= 10\,345.37 \text{ K}. \tag{5.5}$$

T_{SPEC} is calculated using equation 5.3 and the result is shown in Figure 5.7. The average noise temperature of the measurement setup is is calculated as 7 569.8 K over the 50 MHz frequency band centred at 1.575 GHz. With T_{SPEC} now known, the noise temperature of a DUT can be determined with the use of equation 5.2.

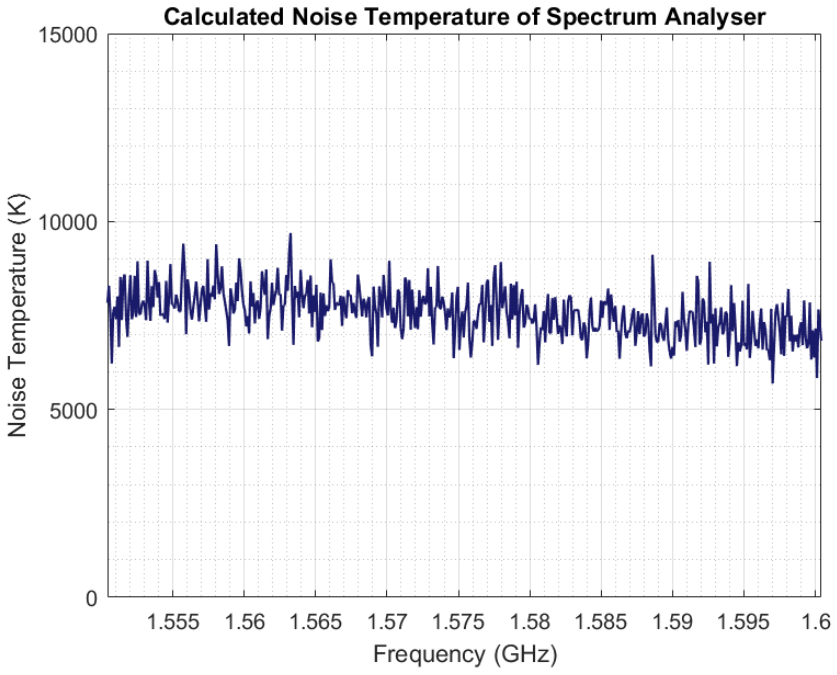

Figure 5.7: Calculated noise temperature of measurement setup.

5.4 Y-factor Measurement of an Active Antenna

To test whether SU-THACO is functional, a Y-factor measurement should be successfully completed. The measurement is deemed successful if two requirements are met. Firstly, if there is a distinguishable difference between the hot and cold measurement. Secondly, the measured result should be within reasonable agreement with the data sheet specification.

A Global Navigation Satellite System (GNSS) receiver antenna is used as the DUT for a Y-factor measurement. The GNSS receiver consists of a patch antenna with an integrated LNA. The receiver centre frequency is 1 575.42 MHz and it has a −3 dB bandwidth of 70 MHz. [49] The receiver system has a gain of 28 dB and noise figure of 1.5 dB. This determines the expected system noise temperature value as 119.63 K.

Firstly, a hot and cold measurement is performed with the DUT, over a bandwidth of 150 MHz to indicate whether the receiver is functional and determine if a clear difference between the hot and cold measurement is apparent. The measurement is performed with SU-THACO and shown in Figure 5.8.

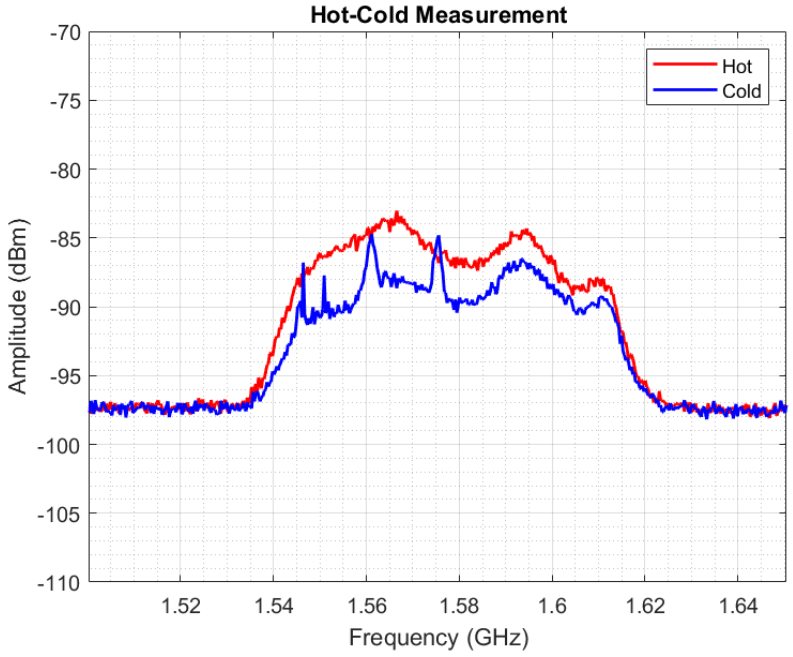

Figure 5.8: Hot-Cold measurement plot with the span of 150 MHz.

It is observed from Figure 5.8 that the receiver is active over its operating frequency. A clear difference between the hot and cold measurement is also observed. At 1.58 GHz the hot measurement is measured as −86.84 dBm and

the cold measurement is −89.74 dBm. There are no external influences observed in the hot measurement, but peaks are present in the cold measurement. The peaks at 1.561 GHz and 1.575 GHz are GNSS or GPS signals, whereas the peaks at 1.546 GHz and 1.551 GHz are attributed to mobile-satellite communication. [50]

The hot and cold measurements are repeated with a bandwidth of 50 MHz, to calculate the system noise temperature of the GNSS receiver within its operating frequency. The measurements over the smaller bandwidth is shown in Figure 5.9.

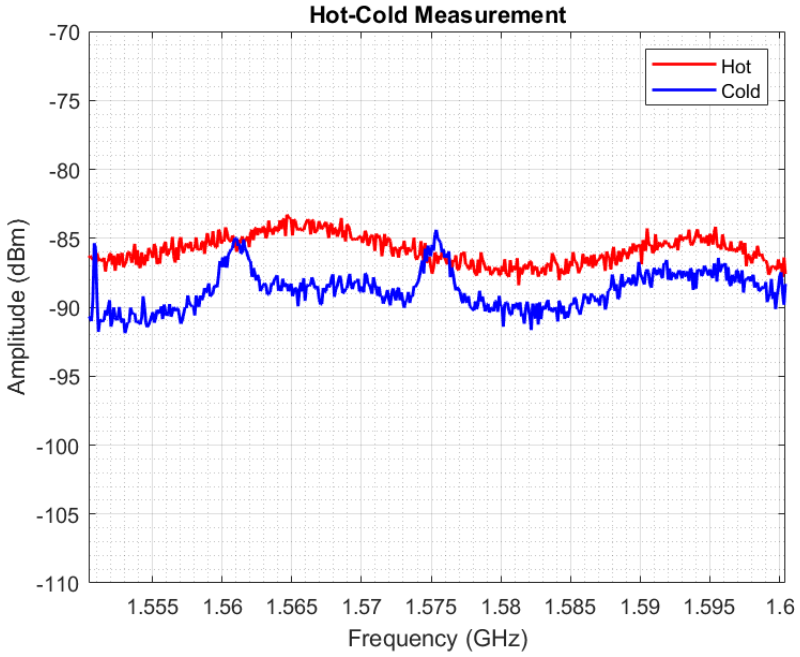

Figure 5.9: Hot-Cold measurement plot with the span of 50 MHz.

The peaks at 1.551 GHz, 1.561 GHz and 1.575 GHz are again observed in the cold measurement shown in Figure 5.9. The RFI signals cause the cold measurement to peak above the hot measurement, for instance at 1.575 GHz the cold measurement is −84.39 dBm whereas the hot measurement is −86.17 dBm. This will cause the Y-factor value to be lower and equal to unity, which will obstruct the accuracy achieved with the measurement.

The Y-factor value is calculated from the hot and cold measurement of the DUT. Figure 5.10 shows the calculated Y-factor values of the DUT over the bandwidth of 50 MHz around the centre frequency. The influence of RFI is observed in the calculated values, where the Y-factor drops below 1 at 1.551 GHz, 1.561 GHz and 1.575 GHz. Even with the presence of RFI signals, a reasonable Y-factor value is obtained in the majority of the frequency band, as shown in Figure 5.10.

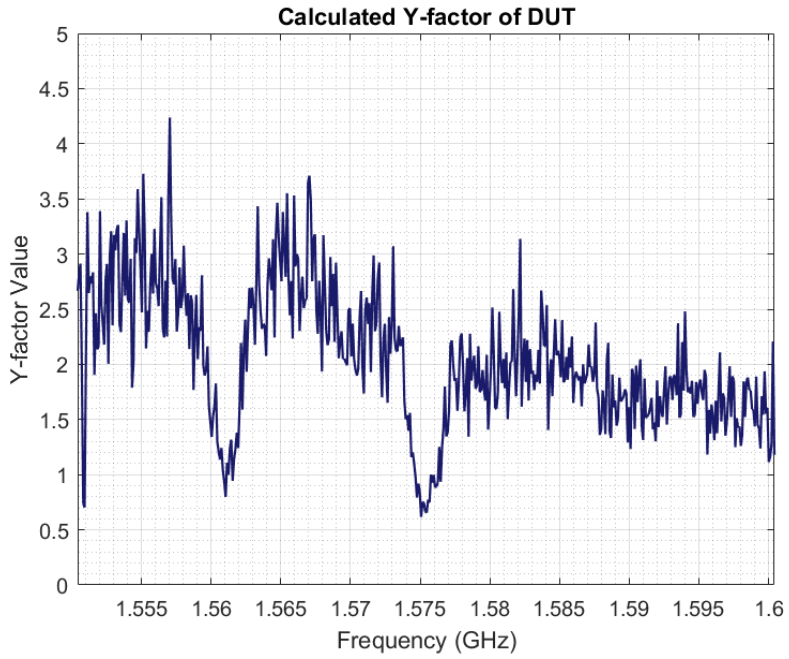

Figure 5.10: Plot of calculated Y-factor value.

With the Y-factor values calculated, the noise temperature of the DUT can be determined by using equation 5.2, where T_{SPEC} is given by the data in Figure 5.7, $G_{\mathrm{DUT}} = 28$ dB and T_{TOT} is calculated as,

$$T_{\mathrm{TOT}} = \frac{T_{\mathrm{hot}} - YT_{\mathrm{cold}}}{Y - 1}. \tag{5.6}$$

T_{hot} for SU-THACO is determined by measuring the physical temperature inside the measurement facility, which determines the noise temperature of the absorber material. The temperature is measured during the hot measurement and is recorded as 25.1°C, which means $T_{\mathrm{hot}} = 298.25$ K. T_{cold} for SU-THACO is assumed to be 12 K in accordance to the simulation for SU-THACO, shown in Figure 4.10.

The noise temperature of the DUT is calculated and the result is shown in Figure 5.11. Due to RFI, the calculated noise temperature plot has values approaching infinity, and negative values. The data is analysed in MATLAB, where a robust averaging technique is applied. The averaging technique assigns lower weights to outliers in the regression, which removes extreme values from the data. The resultant data over the original data is shown in Figure 5.12 and a representation of the averaged data is shown in Figure 5.13.

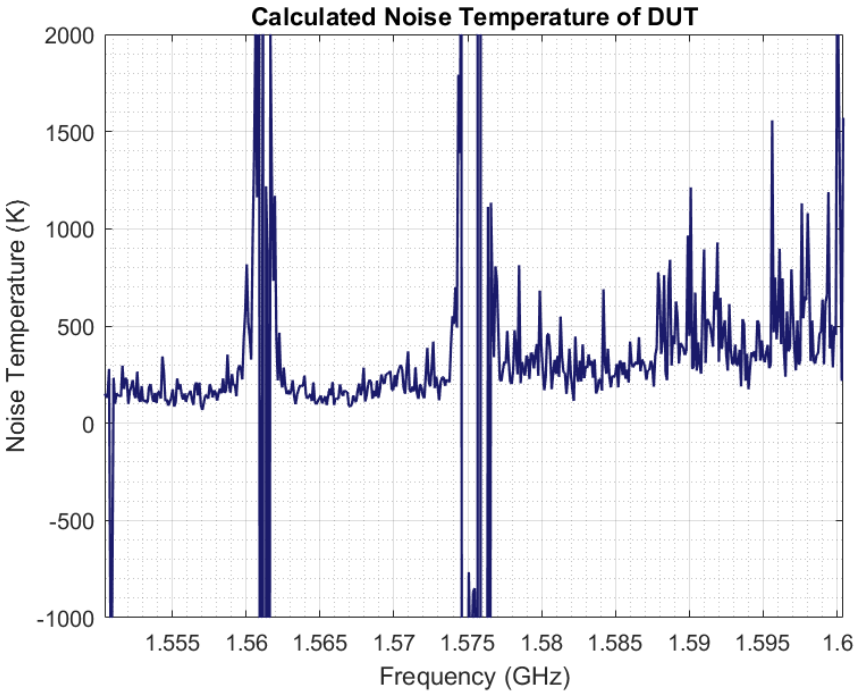

Figure 5.11: Calculated noise temperature of DUT.

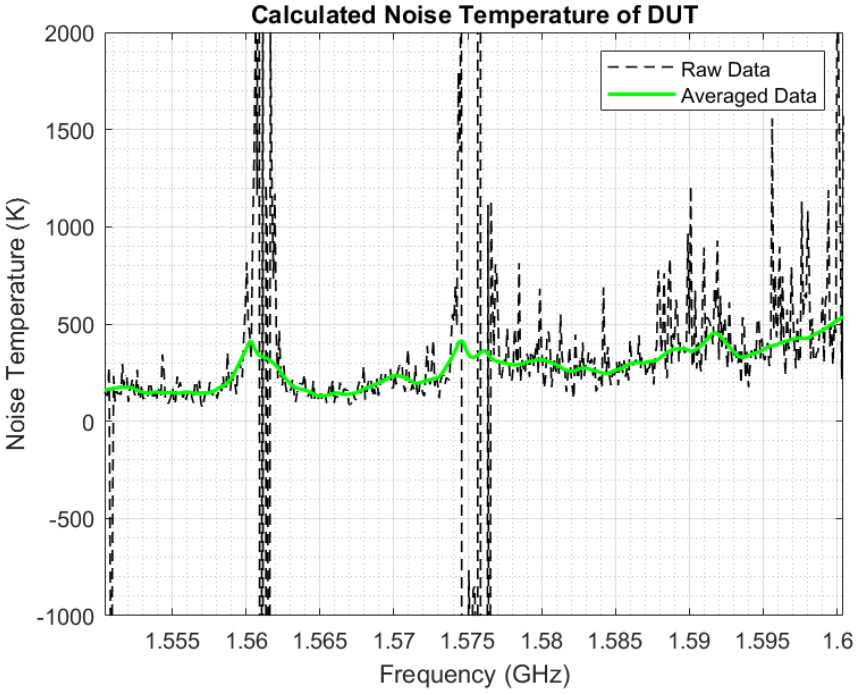

Figure 5.12: Calculated noise temperature of DUT with averaging.

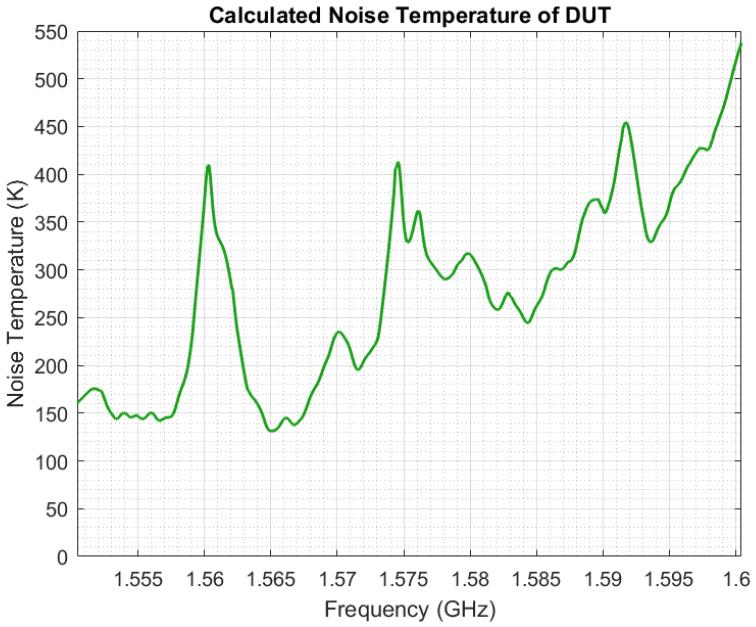

Figure 5.13: Calculated noise temperature of DUT after implementing robust averaging.

The calculated results of Figure 5.13 has a minimum value of 131.2 K at 1.565 GHz and a maximum value of 528.7 K at 1.6 GHz. The minimum value is within 11.57 K of the expected value. To better analyse the data, the noise figure of the DUT is calculated from the noise temperature data in Figure 5.11. The calculated noise figure is shown in Figure 5.14.

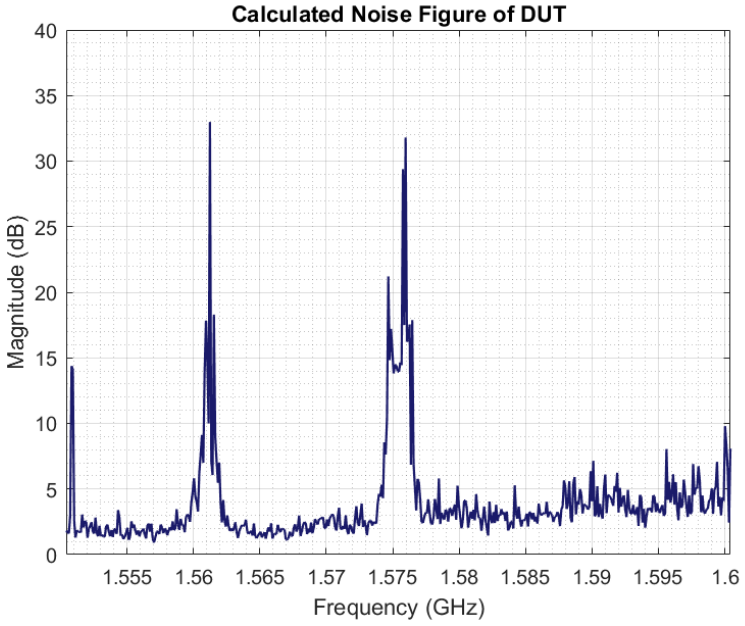

Figure 5.14: Plot of calculated noise figure of DUT.

The noise figure, as shown in Figure 5.14, indicates the peaks due to RFI, but has reasonable values outside of these peaks. The noise figure of the DUT between the peaks at 1.561 GHz and 1.575 GHz is plotted in Figure 5.15, where these values are used to provide an approximation of the noise figure of the DUT.

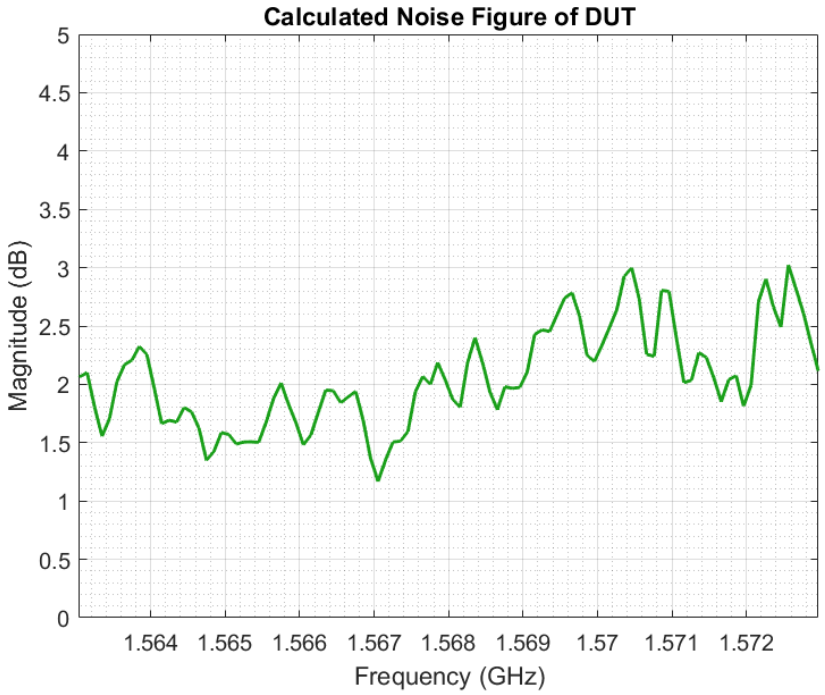

Figure 5.15: Plot of calculated noise figure of DUT over a smaller band.

Figure 5.15 shows the calculated noise figure of the DUT between 1.563 GHz and 1.573 GHz. This data is analysed to give an approximation of the calculated noise figure and noise temperature of the DUT. The maximum value is 3.03 dB at 1.573 GHz, the minimum value is 1.17 dB at 1.567 GHz and the average value is calculated as 2.06 dB.

Thus, the noise figure of the DUT is approximated as 2.06 dB, which is within 0.56 dB of the data sheet specification. In terms of noise temperature, the approximated system noise temperature of the DUT is 176.01 K and is within 39.91 K of the data sheet specification.

5.5 Conclusion

This chapter provides the results obtained with a local Hot-Cold measurement system, that was successfully built on Stellenbosch University grounds. The level of RFI suppression is investigated by measuring the RFI inside and outside of the measurement system with an LPDA. When the roof is open the

RFI is suppressed by 15.19 dBm and with a closed roof, the RFI suppression is 43.99 dBm. Thereafter, hot and cold measurements are done using the developed GUI for SU-THACO. A calibration step is discussed, where the noise temperature of the measurement setup is calculated. After the calibration step is completed, the noise temperature of an active antenna is measured. The measured results show a clear difference between the hot and cold measurement. RFI in the cold measurement obscure the accuracy of the Y-factor calculation. The results are analysed in a frequency band where the RFI influence is minimal. The noise figure of the DUT is calculated as 2.06 dB, which is within 0.56 dB of the data sheet specification. The next chapter draws a conclusion on the implications of these results.

Chapter 6

Conclusion and Recommendations

This thesis was aimed to introduce the reader to a Hot-Cold measurement system, which is used to measure the system noise temperature of active antennas and antenna arrays. The developed system, SU-THACO, operates from 1 GHz to 2 GHz and is situated on the roof of the Electric and Electronic Engineering Department of Stellenbosch University. The facility proved to be user-friendly and could deliver results that were repeatable and capable of yielding repeatable and reliable results.

In chapter 2, an introduction was given to noise found in electronic circuits. Techniques were introduced for measuring the noise temperature of a system. Chapter 3 further elaborated on the system noise temperature of receiver systems used in radio astronomy. A simplified sky brightness temperature model was developed and used to calculate the antenna noise temperature. Chapter 4 gave an introduction to the developed measurement facility at ASTRON, which functioned as a guide for developing a local system on Stellenbosch University grounds.

SU-THACO is a truncated funnel of 1.13 m height and a 20° flare angle, with a removable roof. The system utilises a GUI to perform a Y-factor measurement. An active antenna was measured, and the results were summarized in chapter 5. The developed system delivered sufficient RFI suppression in the target frequency range, with 15.19 dBm suppression when the roof is opened and 43.39 dBm suppression when the roof is closed. The measured system noise temperature of the active antenna was approximated to 176.01 K, or calculated as the noise figure of 2.06 dB. The approximated measured result differs by 0.56 dB with that of the data sheet.

In conclusion, the results show that the developed Hot-Cold measurement system delivers system noise temperature results that have a reasonable agreement with the expected value. This indicates that the use of SU-THACO is adequate to obtain a good approximation of the system noise temperature for design purposes. Future work for this project includes the following developments and recommendations:

- Measure and characterise the noise temperature of additional antenna topologies using SU-THACO: This thesis presented the noise measurements of a commercial single-element active antenna. An in-depth study of the performance and accuracy of SU-THACO for different antenna topologies is suggested. It is also recommended to investigate simulation methods to accurately predict the noise temperature of these devices, to have a simulation to compare the measured results of SU-THACO to.

- Investigate the frequency limit of an outdoor Y-factor measurement: To perform a Y-factor measurement, the hot and cold measurements must be far from each other, for high accuracy in noise temperature prediction. It is recommended to identify the minimum and maximum frequency at which an accurate Y-factor measurement can be performed using SU-THACO. This recommendation includes testing whether measurements below 1 GHz is achievable.

- Improve the mobility of the roof by placing it on tracks: Although the current construction of the roof is user-friendly, it has to be moved by two people. In the future, the condition of the absorber material will also deteriorate due to contact with the edges of the measurement facility. It is recommended to put the absorber material and roof on a track so that it can hover over the measurement facility, and switch easier between the hot and cold states.

Bibliography

[1] "SQUARE KILOMETRE ARRAY." [Online]. Available: www.skatelescope.org

[2] E. E. M. Woestenburg, L. Bakker, M. Ruiter, M. V. Ivashina, and R. H. Witvers, "THACO, a Test Facility for Characterizing the Noise Performance of Active Antennas Arrays."

[3] G. C. Medellin, "Antenna Noise Temperature Calculation," *SKA Memo 95*, pp. 1–12.

[4] K. F. Warnick, R. Maaskant, M. V. Ivashina, D. B. Davidson, and B. D. Jeffs, "High-Sensitivity Phased Array Receivers for Radio Astronomy," *Proceedings of the IEEE*, vol. 104, no. 3, pp. 607–622, 2016.

[5] W. T. Sullivan, *Classics in Radio Astronomy*. Dordrecht:Holland / Bostan:U.S.A / London:England: D. Reidel Publishing Company, 1981.

[6] K. G. Jansky, "Directional studies of atmospherics at high frequencies," *Proceedings of the Institute of Radio Engineers*, vol. 20, no. 12, pp. 1920–1932, 1932.

[7] ——, "Radio waves from outside the solar system," *Nature*, vol. 132, no. 3323, pp. 66–66, 1933.

[8] W. T. Sullivan, Ed., *The early years of Radio Astronomy: Reflections fifty years after Jansky's discovery*. Cambridge: Cambridge University Press, 1984.

[9] SKA, "Technical Information: The Telescope." [Online]. Available: https://www.skatelescope.org/technical/info-sheets/

[10] Ruiter, M.; van Cappellen, W.; van der Wal, E.; Arts, M.; van den Brink, R.; Visser, K., "Development of a Vivaldi Tile for SKA Mid Frequency Aperture Array."

[11] M. Ruiter and E. Van Der Wal, "EMBRACE, a 10 000 element next generation aperture array telescope," *European Microwave Week 2009,*

EuMW 2009: Science, Progress and Quality at Radiofrequencies, Conference Proceedings - 39th European Microwave Conference, EuMC 2009, no. October, pp. 326–329, 2009.

[12] P. Benthem and G. W. Kant, "EMBRACE: Results from an aperture array for radio astronomy," *Proceedings of 6th European Conference on Antennas and Propagation, EuCAP 2012*, pp. 629–633, 2012.

[13] W. A. Van Cappellen and L. Bakker, "APERTIF: Phased array feeds for the Westerbork Synthesis Radio Telescope," *IEEE International Symposium on Phased Array Systems and Technology*, pp. 640–647, 2010.

[14] W. A. Van Cappellen, L. Bakker, and T. A. Oosterloo, "Experimental results of the APERTIF phased array feed," *2011 30th URSI General Assembly and Scientific Symposium, URSIGASS 2011*, pp. 1–4, 2011.

[15] E. E. Woestenburg and K. F. Dijkstra, "Noise characterization of a phased array tile," *Conference Proceedings - 33rd European Microwave Conference, EuMC 2003*, vol. 1, no. 2, pp. 363–366, 2003.

[16] E. E. Woestenburg, L. Bakker, and M. V. Ivashina, "Experimental results for the sensitivity of a low noise aperture array tile for the SKA," *IEEE Transactions on Antennas and Propagation*, vol. 60, no. 2 PART 2, pp. 915–921, 2012.

[17] J. G. de Vaate, L. Bakker, and R. Witvers, "Active antenna design and characterization," *Proceedings of Science*, vol. 132, no. November, pp. 173–176, 2009.

[18] C. K. Miller, W. C. Daywitt, and M. G. Arthur, "Noise Standards, Measurements, and Receiver Noise Definitions," *Proceedings of the IEEE*, vol. 55, no. 6, pp. 865–877, 1967.

[19] P. Z. Peebles Jr, *Probability, random variables, and random signal principles*. McGraw Hill Book Company, 1987.

[20] W. Schottky, "Über spontane stromschwankungen in verschiedenen elektrizitätsleitern," *Annalen der physik*, vol. 362, no. 23, pp. 541–567, 1918.

[21] J. B. Johnson, "Electronic Noise: the first two decades," *IETE Journal of Education*, vol. 10, no. 4, pp. 157–162, 1969.

[22] ——, "Thermal agitation of electricity in conductors," *Nature*, vol. 119, no. 2984, pp. 50–51, 1927.

[23] B. Oliver, "Thermal and quantum noise," *Proceedings of the IEEE*, vol. 53, no. 5, pp. 436–454, 1965.

[24] M. S. Keshner, "1/f Noise," *Proceedings of the IEEE*, vol. 70, no. 3, pp. 212 – 218, 1982.

[25] H. W. Ott, *Electromagnetic Compatibility Engineering.* John Wiley & Sons, Inc., 2009.

[26] D. M. Pozar, *Microwave Engineering*, 4th ed. Hoboken: John Wiley & Sons, Inc., 2012.

[27] H. Friss, "Noise Figures of Radio Receivers," *IEE Review*, vol. 34, no. 9, p. 362, 1988.

[28] J. G. Kreer *et al.*, "IRE Standards on Methods of Measuring Noise in Linear Twoports," *Proceedings of the IRE*, vol. 48, no. 1, pp. 60–68, 1960.

[29] Microwaves101, "Noise Figure One and Two, Friis and IEEE." [Online]. Available: https://www.microwaves101.com/encyclopedias/noise-figure-one-and-two-friis-and-ieee

[30] J. Fernandez, "A noise-temperature measurement system using a cryogenic attenuator," *TMO progress report*, vol. 15, pp. 42–135, 1998.

[31] IEEE Antennas and Propagation Society, "IEEE Standard for Definitions of Terms for Antennas," *IEEE Standards Association*, vol. 145, 2013.

[32] F. Ulaby, R. Moore, and A. Fung, *Microwave Remote Sensing.* Addison-Wesley Publishing Company, 1981, vol. I, ch. 4–5.

[33] J. Waters, "Absorption and Emission by Atmospheric Gases," in *Methods of Experimental Physics.* New York: Academic Press, 1976, vol. 12B, pp. 142–176.

[34] P. W. Rosenkranz, "Shape of the 5 mm Oxygen Band in the Atmosphere," *IEEE Transactions on Antennas and Propagation*, vol. 23, no. 4, pp. 498–506, 1975.

[35] M. V. Ivashina, R. Maaskant, and B. Woestenburg, "Equivalent system representation to model the beam sensitivity of receiving antenna arrays," *IEEE Antennas and Wireless Propagation Letters*, vol. 7, pp. 733–737, 2008.

[36] G. J. Hovey, R. Messing, A. G. Willis, and B. Veidt, "An Automated System for Measurement of Sensitive Microwave Radiometers," *Proceedings - ANTEM 2018: 2018 18th International Symposium on Antenna Technology and Applied Electromagnetics*, vol. 2018-Augus, pp. 1–2, 2018.

[37] B. C. Enthoven and R. Maaskant, "Design of a Hot-Cold Test Facility," *ASTRON Mechanical Design Engineering*, vol. 1, no. June, pp. 1–23, 2007.

[38] "Aluminum Uses in Electrical Shielding - Clinton Aluminum." [Online]. Available: https://www.clintonaluminum.com/aluminum-uses-in-electrical-shielding/

[39] ICASA, "Draft Terrestrial Broadcating Frequency Plan," pp. 23–37, 2008. [Online]. Available: https://www.gov.za/sites/default/files/gcis{_}document/201409/315011272b.pdf

[40] Emerson & Cuming Anechoic Chambers, "Product Information Eccosorb® VHP-NRL," vol. 01/2, 2010/04.

[41] UVOX, "Beryllium-Copper Fingerstrip," *Technical Datasheet*, vol. 44, no. 0, pp. 55–57. [Online]. Available: www.uvox.co.uk

[42] RS-PRO, "Datasheet: EPDM Black Rubber Sealing Strip," p. 6087.

[43] Times Microwave Systems, "LMR-400," *TMS-COAX*, no. 800, pp. 22–25. [Online]. Available: www.timesmicrowave.com

[44] RS Components, "Amphenol RF 50Ω Straight Panel Mount SMA Connector Bulkhead Fitting, jack." [Online]. Available: https://za.rs-online.com/web/p/coaxial-connectors/1440952

[45] Rohde and Schwarz, "Spectrum Analysers FSEx," *Test Equipment Solutions Datasheet*, vol. 44, no. 0, pp. 0–17.

[46] "South African Table of Frequency Allocations." [Online]. Available: https://www.icasa.org.za/uploads/files/ITU-Reference-Review-the-Radio-Frequency-Band-Plan-31264.pdf

[47] Rohde and Schwarz, "Better system sensitivity through preamplifiers," *News letter*, vol. II, no. 178, pp. 41–45, 2003.

[48] Keysight Technologies, "Keysight 346A/B/C Noise Source," *Operating and Service Manual*, pp. 1–87.

[49] Aliexpress, "GNSS receiver antenna." [Online]. Available: https://www.aliexpress.com/item/32804278735.html?spm=a2g0o.productlist.0.0.3ef596076D2fGs%7B&%7Dad%7B_%7Dpvid=202009150322114818620275755000001577014%7B_%7D1%7B&%7Ds=p

[50] "South African Table of Frequency Allocations." [Online]. Available: https://www.icasa.org.za/uploads/files/ITU-Reference-Review-the-Radio-Frequency-Band-Plan-31264.pdf

Appendices

Appendix A: How to use the SU-THACO GUI

Step 1 Complete the measurement setup and plug in the GPIB-USB cable into the laptop. Open the NIMax application to confirm that the connection is active.

Step 2 Open MATLAB R2018b and run GUI.mlapp.

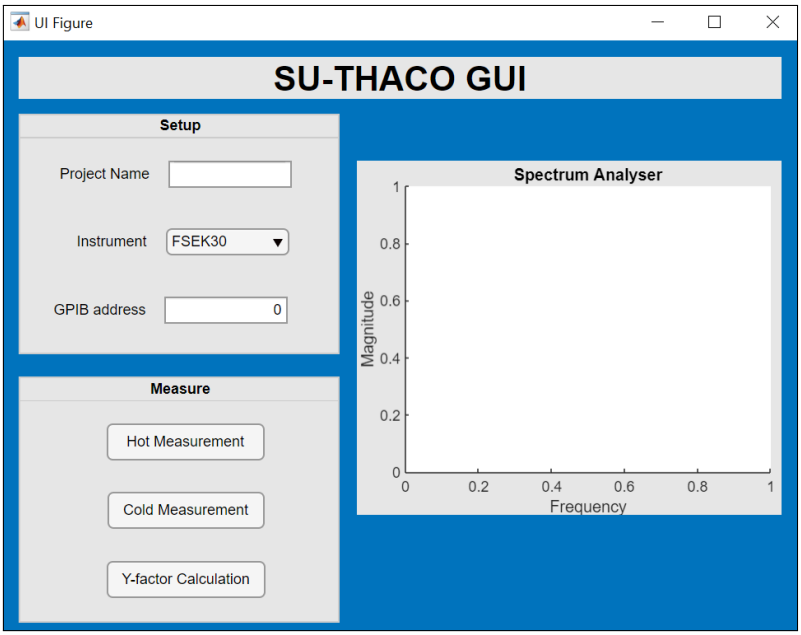

Figure 1: SU-THACO GUI opened on MATLAB.

Step 3 Fill in the required data in the **Setup** field.

The instrument choice is between the FSEK30, HP8590 and HP8562 spectrum analysers available in the Microwave laboratory of Stellenbosch University. The GPIB address is specified in NIMax.

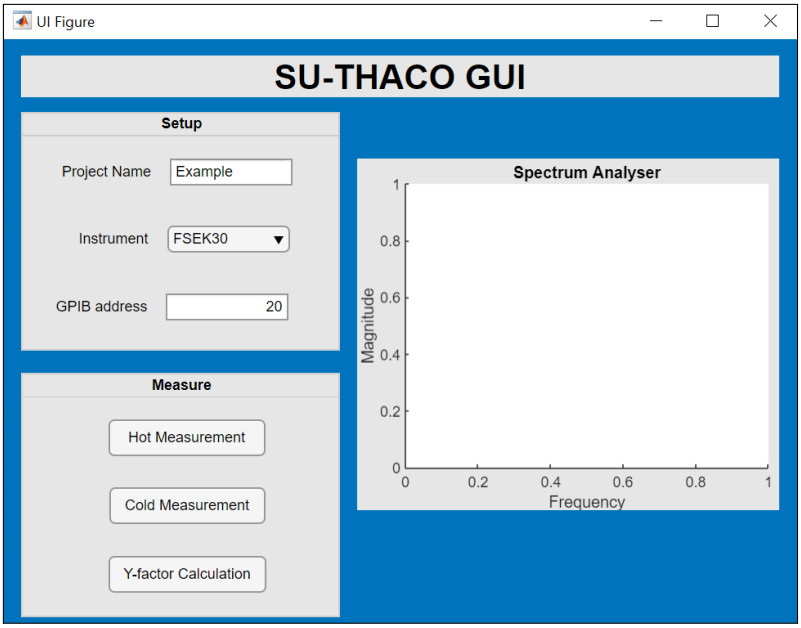

Figure 2: Example of the filled in setup field.

Step 4 Make sure the roof is closed, and press the **Hot Measurement** button to record the hot measurement data.

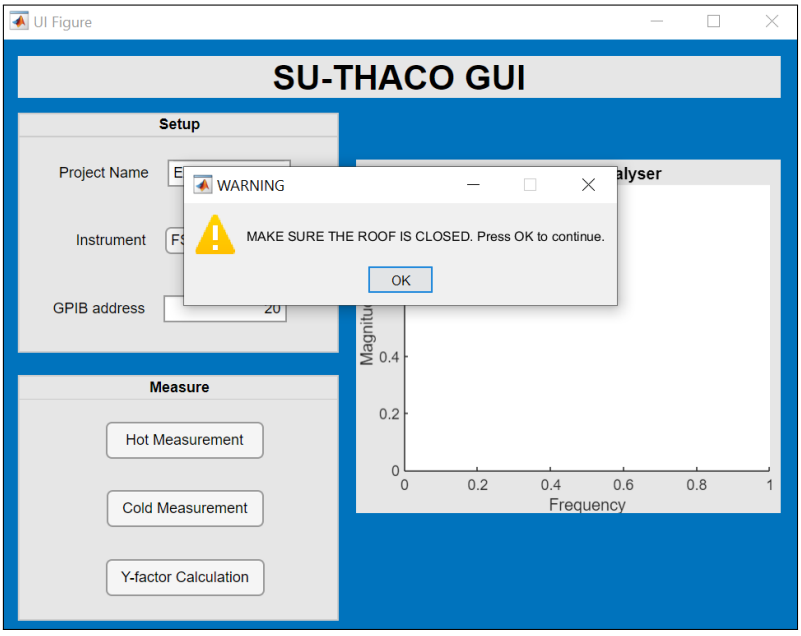

Figure 3: Hot measurement with SU-THACO GUI.

Step 5 Remove the roof from the facility, and press the **Cold Measurement** button to record the cold measurement data.

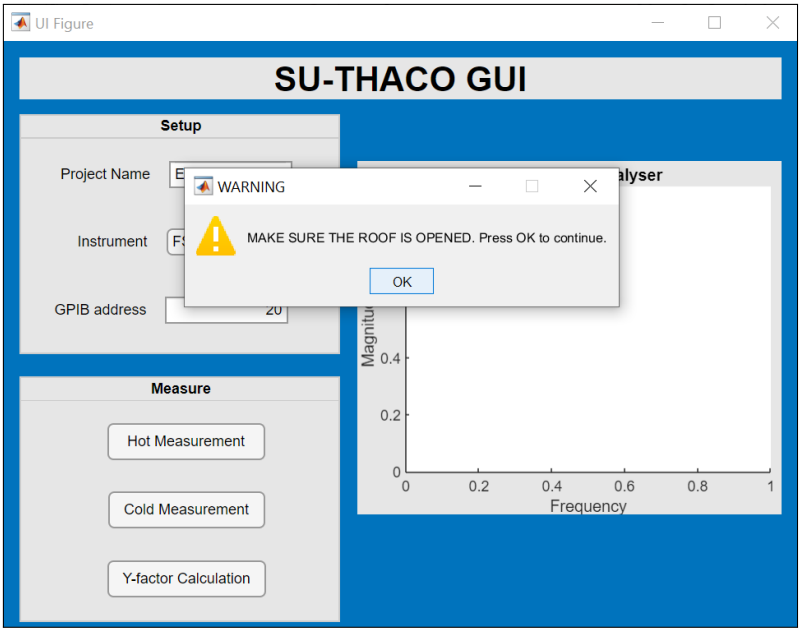

Figure 4: Cold measurement with SU-THACO GUI.

Step 6 Use the **Y-Factor Calculation** button to view the calculated Y-factor for the hot and cold measurement.

Step 7 To repeat steps 3 to 5, change the **Project Name**, for examlpe adding an incrementation, otherwise the data of the previous measurement is overwritten.

Appendix B: Additional Images of SU-THACO

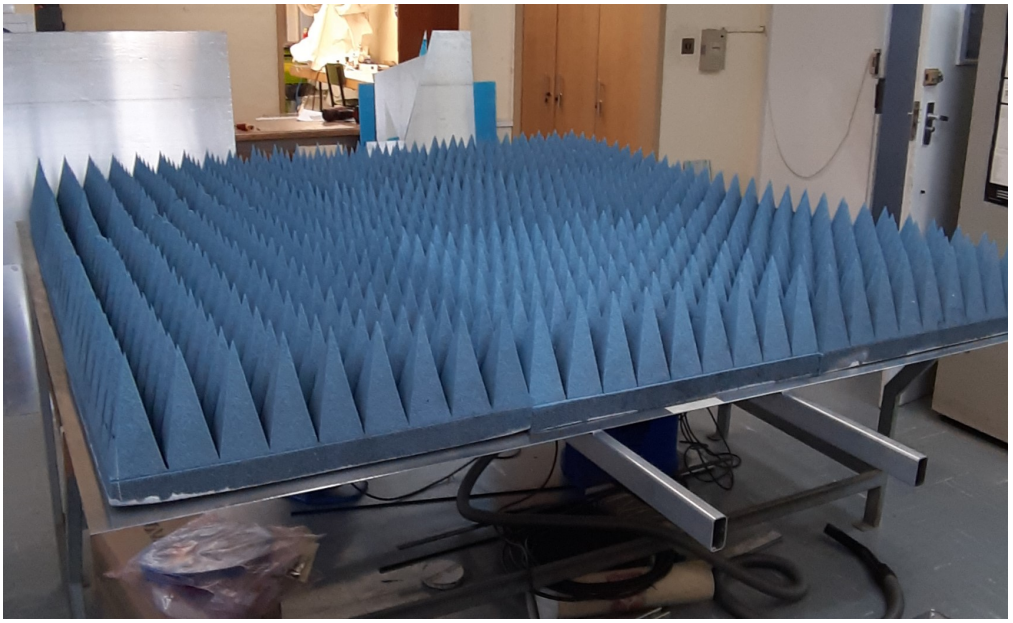

Figure 5: The assembly of absorber material on the roof of SU-THACO.

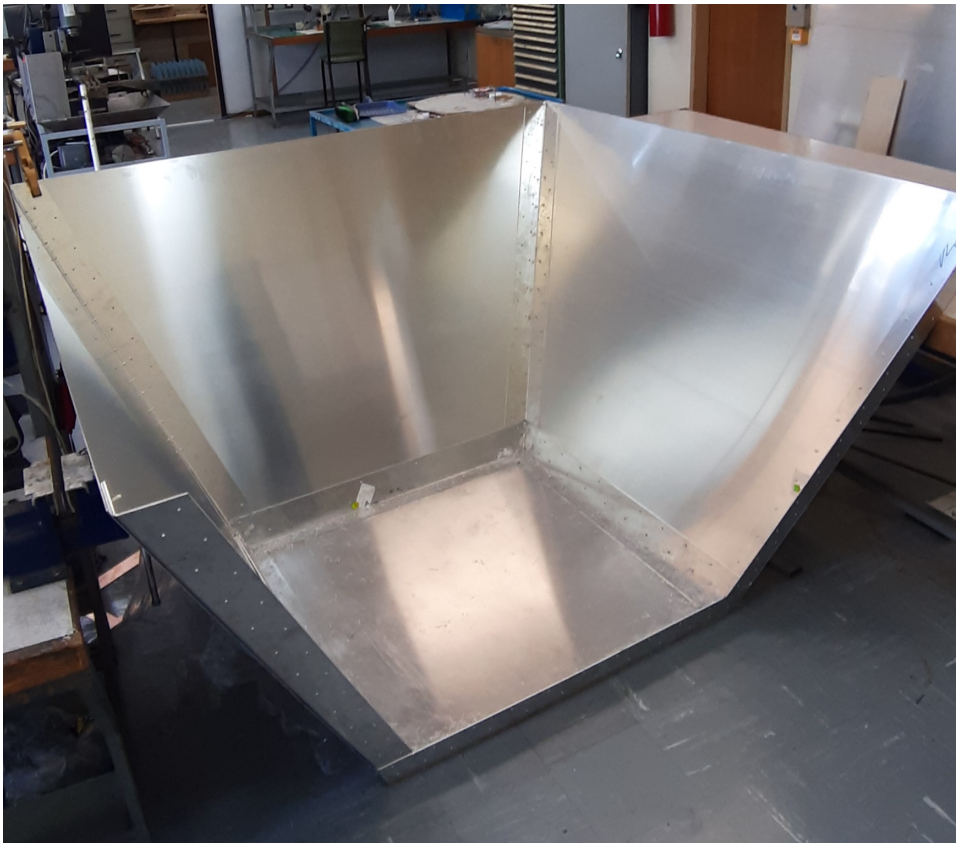

Figure 6: The assembly of SU-THACO inside the engineering workshop at Stellenbosch University.

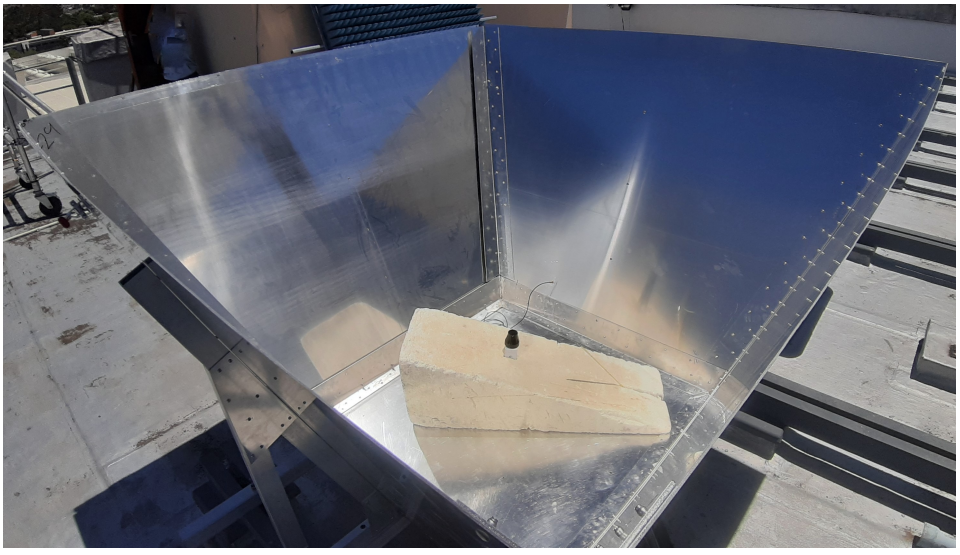

Figure 7: The active antenna inside SU-THACO with the roof opened.

Figure 8: The SMA connection on the outside of the SU-THACO facility.